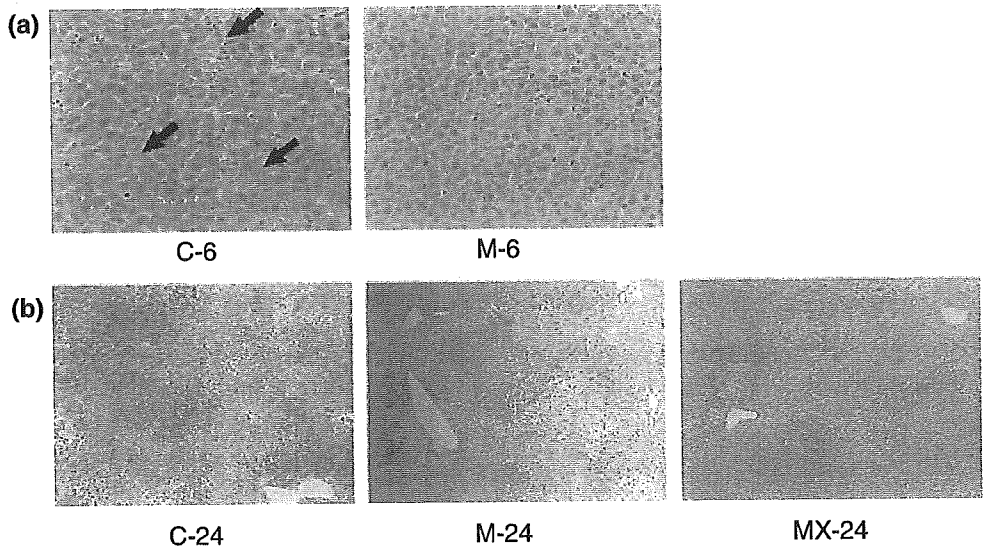

Figure 3 Representative histologic findings in the excised livers at 6 h and 24 h after reperfusion. (a) At 6 h after reperfusion, focal necrosis (arrows) and sinusoidal congestion were observed in the control group (group C-6) but not in the MCI-186-treated group (group M-6). Original magnification ×400. (b) At 24 h after reperfusion, spotty necrosis, ballooning of parenchymal cells, and more severe sinusoidal congestion were seen in the control group (group C-24) and also in the MCI-186-treated group (group M-24) but not in group MX-24 (original magnification ×100).

Table 2. Numerical degree of histologic damage according to the criteria advocated by Suzuki *et al.* (28). Congestion, vacuolization, and necrosis in liver tissue were estimated.

Groups	Congestion	Vacuolization	Necrosis
C-6	3.67 ± 0.21	0.67 ± 0.21	3.33 ± 0.21
M-6	2.33 ± 0.33*	0.50 ± 0.22	2.33 ± 0.21*
C-24	3.17 ± 0.17	3.50 ± 0.22	3.83 ± 0.17
M-24	2.83 ± 0.17	2.33 ± 0.21*	3.67 ± 0.21
MX-24	1.67 ± 0.21*,**	1.83 ± 0.31*	2.50 ± 0.22*,**

*$P < 0.05$ compared with group C.
**$P < 0.05$ compared with group M-24.

C-6, but those of the mRNAs for chemokines CINC-2, MIP-2, MCP-1 and MIP-1α were significantly decreased in group M-6. Expression of MIP-1β mRNA was not suppressed by MCI-186 at any time point. Figure 6c shows the expression of cytokine and chemokine mRNAs at 24 h. Expression was still high in group C-24, and CINC-2 and MIP-2 mRNA expression was suppressed significantly in group M-24. However, no suppression of IL-1, MCP-1, MIP-1α, and MIP-1β mRNA expression was evident. In group MX-24, the expression levels of mRNAs for all cytokines and chemokines were low. The differences in the expression levels of IL-1, MCP-1, MIP-1α and MIP-1β mRNAs were significant in comparison with groups C-24 and M-24.

We also investigated ICAM-1 mRNA expression at 6 h, as shown in Fig. 7. ICAM-1 mRNA expression was high 6 h after reperfusion (group C-6) and gradually decreased thereafter. The expression was significantly reduced in group M-6.

Discussion

We have investigated the usefulness of MCI-186 for the prevention of hepatic warm IRI in a rat model. The results demonstrate that administration of MCI-186 before reperfusion suppressed IRI in the acute phase, but did not result in sufficient suppression in the subacute phase. Additional administration of MCI-186 12 h after reperfusion also suppressed IRI in the subacute phase. This additional administration is presumably necessary because of the short half-life of MCI-186 and the multistep nature of hepatic IRI [1–9].

Free radicals are one of the important factors responsible for hepatic IRI [2–5,29], and several investigators have reported that free radical scavengers attenuate hepatic IRI [3–5,30–35]. Nevertheless, no such scavenger has been used clinically to date recently. MCI-186 is now used clinically and is beneficial after cerebral infarction. There have been several reports describing beneficial effect of MCI-186 on hepatic IRI, e.g. it attenuates liver injury at acute phase [22], it protects against mitochondrial injury [23] and it ameliorates cold IRI [20] or warm IRI [21] in isolated liver perfusion model using Krebs–Henseleit solution. However, none of these studies have focused on the effects of this reagent against various chemical

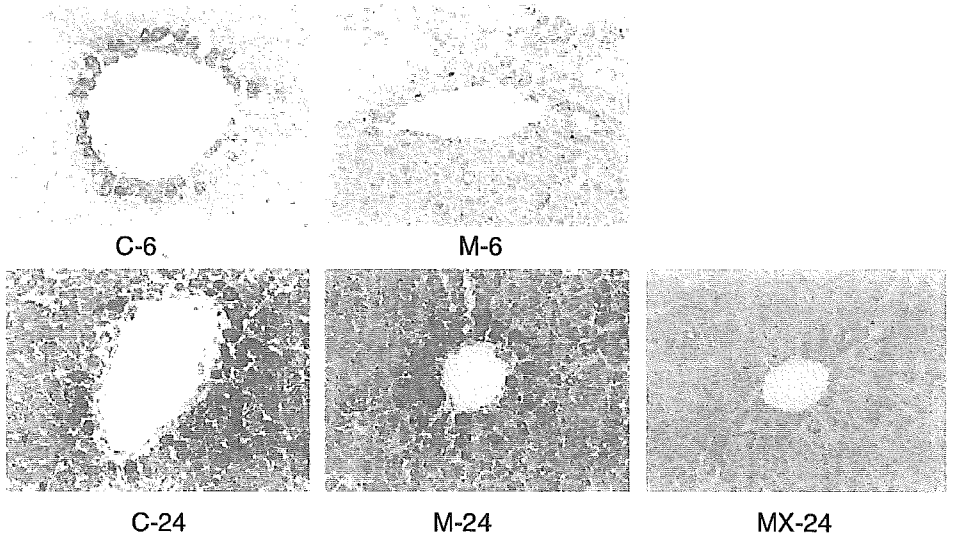

Figure 4 Representative findings of lipid peroxidation immunostaining with monoclonal antibody against 4-hydroxy-2-nonenal (4-HNE) modified proteins in rat livers at 6 h and 24 h after reperfusion. In groups C-6 and C-24, 4-HNE-positive cells were observed. Although 4-HNE staining was faint in group M-6, the number of 4-HNE-positive cells in group M-24 was comparable with that in group C-24. The number of 4-HNE-positive cells was decreased in group MX-24, compared with groups C-24 and M-24 (original magnification ×400).

mediators such as free radicals, cytokines and chemokines, inflammatory cells, adhesion molecules, and also against histologic damage in hepatic IRI model *in vivo*.

The ODFRs activate monocytes (resident or free) and induce nuclear factor κB in hepatic IRI, causing hepatic injury in the early phase [8,12,31,36–38]. TNF-α and IL-1β are potent proinflammatory cytokines secreted mainly by Kupffer cells during hepatic IRI [2–6,8,39,40]. These cytokines induce IL-8 and CINC-2 synthesis [4,41] and upregulate the expression of adhesion molecules such as Mac-1 or ICAM-1 [3,4]. TNF-α also induces chemokines such as epithelial neutrophil-activating protein 78, which plays an important role in neutrophil chemotaxis and activation, and stimulates ODFR production by Kupffer cells [2,4,7,42,43]. IL-1β induces Kupffer cells to produce TNF-α, upregulates ODFR production by neutrophils [4], and also upregulates the expression of nuclear factor κB and CXC chemokines [8]. In this study, the expression of TNF-α and IL-1β was elevated in the early phase after reperfusion, and attenuated in the MCI-186-treated groups.

MCP-1, MIP-1α and MIP-1β are CC chemokines, which exert a chemotactic effect on monocytes and T cells [10–13]. The expression levels of MCP-1 and MIP-1α were reduced in the MCI-186-treated group 3 h and 6 h (acute phase) after reperfusion. MCI-186 reduced monocyte infiltration into the liver, and this might have resulted from suppressed expression of CC chemokines. In the early phase of hepatic IRI, ODFR-stimulated Kupffer cells release MCP-1 [12], upregulates ICAM-1 expression on endothelial cells *in vitro* [44]. Up-regulation of ICAM-1 is one of the important factors involved in the pathogenesis of neutrophil-induced hepatic IRI [45]. These correlations appear to be supported by the present *in vivo* data indicating that suppression of MCP-1 and ICAM-1 expression in the MCI-186-treated groups led to a decrease in monocyte and neutrophil infiltration.

Similar mRNA expression patterns were also observed for members of the CXC chemokine superfamily (CINC-2 and MIP-2). CXC chemokines have potent chemotactic effects on neutrophils. Kupffer cells produce CINC when stimulated with ODFR generated by hypoxanthine and xanthine oxidase [2,3,41], while CINC-2 production can be reduced with a calcium channel blocker [41]. The level of CINC-2 is increased for several hours after reperfusion in rat liver IRI models [2,41]. MIP-2 is also upregulated in early hepatic or renal IRI and has an important role in neutrophil recruitment and organ injury [7,9,13]. Our results indicate that CINC-2 and MIP-2 levels were elevated in the early phase of IRI in the control groups, and we suspect a correlation between the expression of CXC chemokines and neutrophil infiltration. This inference is supported by the observation that both CXC chemokine expression and neutrophil infiltration were suppressed in the MCI-186-treated groups.

In our study, single administration of MCI-186 did not have attenuated infiltration of neutrophils or macrophages in the subacute phase presumably because of its short

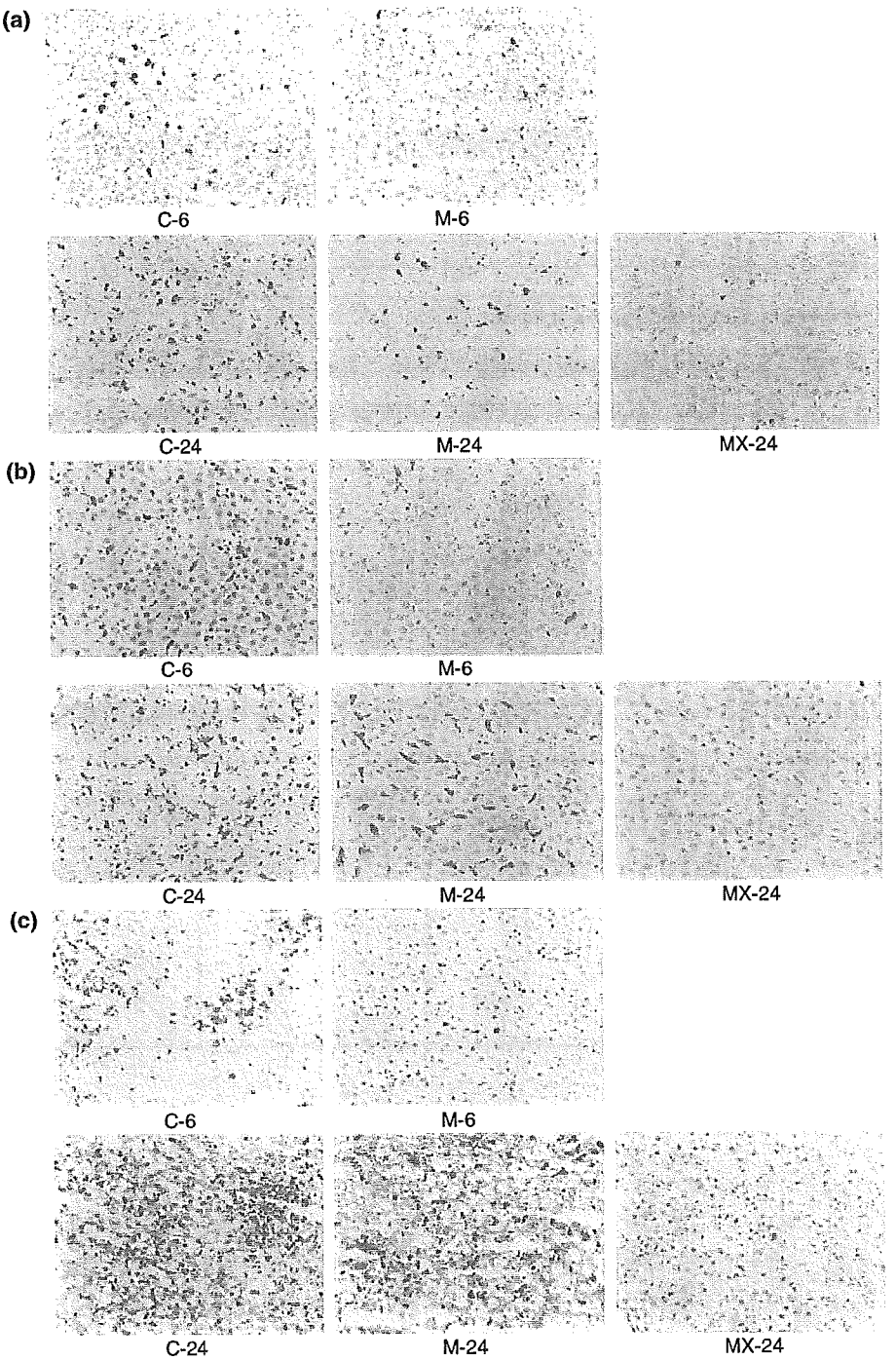

Figure 5 Immunohistochemistry for inflammatory cells in the liver tissues. (a) ED-1-positive cells (resident macrophages). (b) ED-2-positive cells (free macrophages). (c) Neutrophils. The numbers of ED-1- and ED-2-positive cells in the ischemic lobes were increased in group C-6 but absent in group M-6. In group M-24, the numbers of ED-1- and ED-2-positive cells in the ischemic lobes were increased. In group MX-24, the number of macrophages was markedly reduced. Infiltration of neutrophils into the sinusoids was observed in groups C-6 and C-24. Infiltration was suppressed in group M-6, but not in group M-24. In group MX-24, infiltration of neutrophils into sinusoids was demonstrably reduced (original magnification ×400).

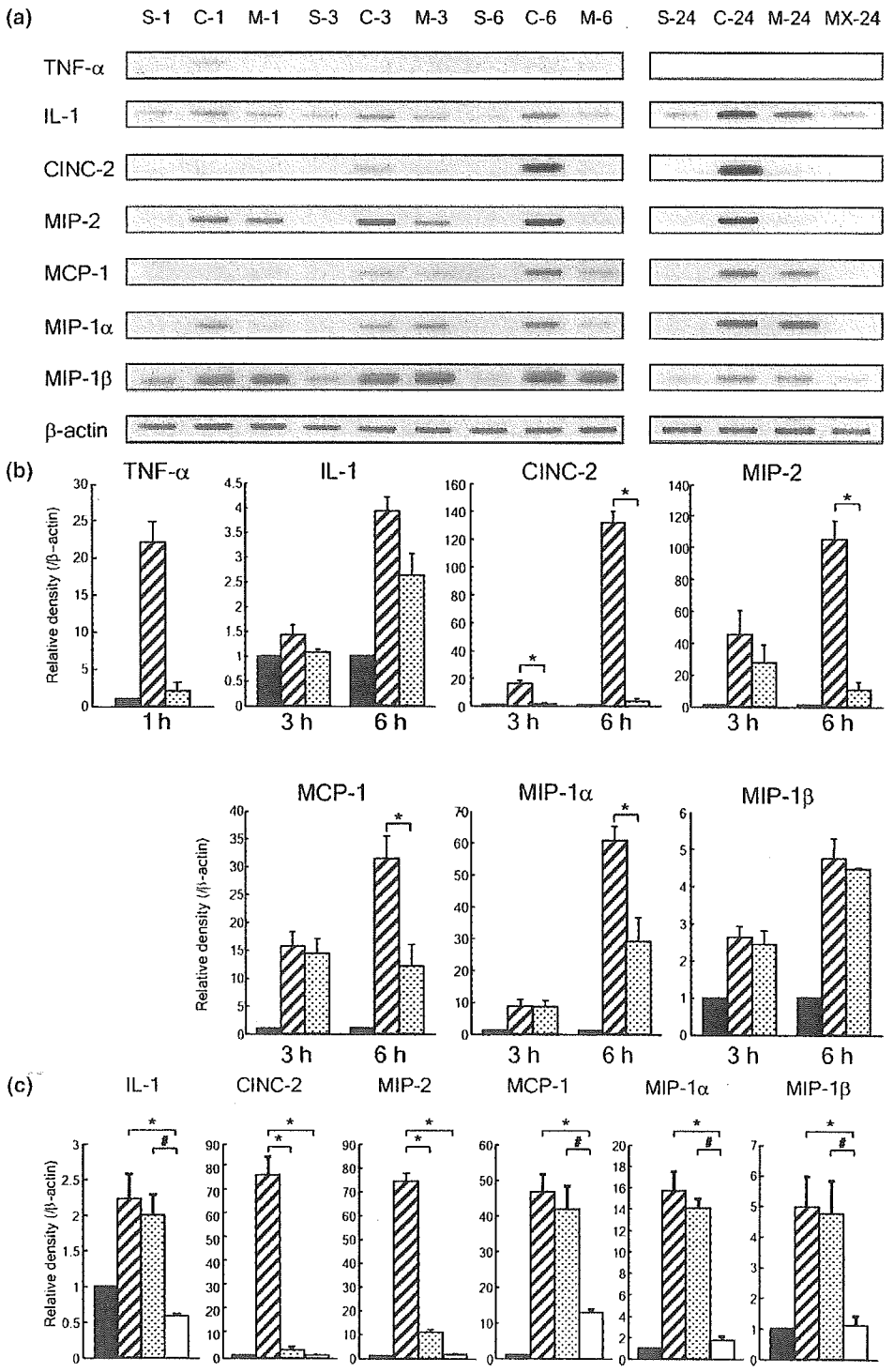

Figure 6 (a) Expression of cytokine and chemokine mRNAs in ischemic lobes of rats. (b) Semiquantification of cytokines and chemokines in the acute phase. (c) Semiquantification of cytokine and chemokines in the subacute phase. Analysis of bands for β-actin and cytokines or chemokines is shown, and the data represent the ratio from five different animals. The expression of cytokines and chemokines was high in group C, but attenuated in group M and group MX. Data represent mean ± SEM. *$P < 0.05$ compared with group C; #$P < 0.05$ compared with group M-24. ■, group S; ▨,group C; ▩, group M; □, group MX.

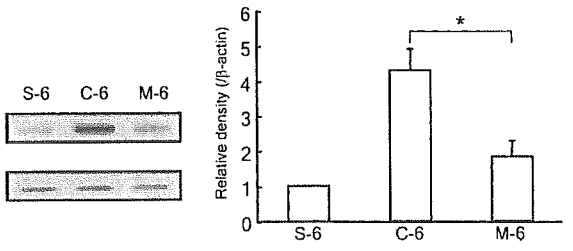

Figure 7 Level of expression of intercellular adhesion molecule (ICAM)-1 mRNA in the ischemic lobe at 6 h after reperfusion. Analysis of bands for ICAM-1 and β-actin is shown, and the data represent the ratio from five different animals. The expression of ICAM-1 was high in group C, but attenuated in group M. Data represent mean ± SEM. $*P < 0.05$ compared with group C.

half-life and the timing of injection [the half-life of MCI-186 is 0.17 h ($t_{1/2}\alpha$) and 0.81–0.85 h ($t_{1/2}\beta$) at a dose of 1.5 mg/kg in clinical laboratory tests] [27]. These pharmacokinetic data suggested the need for a second experiment that included additional administration of MCI-186 (group MX-24). As a result, additional administration of MCI-186 at 12 h after reperfusion suppressed IRI with attenuation of ODFRs and other mediators in the subacute phase.

In summary, MCI-186 attenuates liver injury *in vivo* in a rat warm IRI model, suggesting that this clinically applicable free radical scavenger has the potential to attenuate liver dysfunction in patients after hepatic resection and liver transplantation.

Acknowledgements

This work was supported in part by a grants-in-aid for scientific research from the Ministry of Education, Culture, Sports, Science and Technology of Japan (08457297, 09877243, 13470150), the Takeda Medical Foundation, and the Vehicle Racing Commemorative Foundation. We would like to thank Ms K. Misawa for technical assistance.

References

1. Jaeschke H, Farhood A, Smith CW. Neutrophils contribute to ischemia/reperfusion injury in rat liver *in vivo*. *FASEB J* 1990; **4**: 3355.
2. Teoh NC, Farrell GC. Hepatic ischemia reperfusion injury: pathogenic mechanisms and basis for hepatoprotection. *J Gastroenterol Hepatol* 2003; **18**: 891.
3. Jaeschke H. Molecular mechanisms of hepatic ischemia–reperfusion injury and preconditioning. *Am J Physiol Gastrointest Liver Physiol* 2003; **284**: G15.
4. Serracino-Inglott F, Habib NA, Mathie RT. Hepatic ischemia–reperfusion injury. *Am J Surg* 2001; **181**: 160.
5. Fondevila C, Busuttil RW, Kupiec-Weglinski JW. Hepatic ischemia/reperfusion injury – a fresh look. *Exp Mol Pathol* 2003; **74**: 86.
6. Zwacka RM, Zhang Y, Halldorson J, Schlossberg H, Dudus L, Engelhardt JF. CD4(+) T-lymphocytes mediate ischemia/reperfusion-induced inflammatory responses in mouse liver. *J Clin Invest* 1997; **100**: 279.
7. Lentsch AB, Yoshidome H, Cheadle WG, Miller FN, Edwards MJ. Chemokine involvement in hepatic ischemia/reperfusion injury in mice: roles for macrophage inflammatory protein-2 and KC. *Hepatology* 1998; **27**: 1172.
8. Kato A, Gabay C, Okaya T, Lentsch AB. Specific role of interleukin-1 in hepatic neutrophil recruitment after ischemia/reperfusion. *Am J Pathol* 2002; **161**: 1797.
9. Martinez-Mier G, Toledo-Pereyra LH, McDuffie JE, Warner RL, Ward PA. Neutrophil depletion and chemokine response after liver ischemia and reperfusion. *J Invest Surg* 2001; **14**: 99.
10. Luster AD. Chemokines–chemotactic cytokines that mediate inflammation. *N Engl J Med* 1998; **338**: 436.
11. Baggiolini M. Chemokines and leukocyte traffic. *Nature* 1998; **392**: 565.
12. Yamaguchi Y, Matsumura F, Liang J, *et al.* Neutrophil elastase and oxygen radicals enhance monocyte chemoattractant protein-1 expression after ischemia/reperfusion in rat liver. *Transplantation* 1999; **68**: 1459.
13. Martinez-Mier G, Toledo-Pereyra LH, McDuffie JE, *et al.* Exogenous nitric oxide down-regulates MIP-2 and MIP-1 α chemokines and MAPK p44/42 after ischemia and reperfusion of the rat kidney. *J Invest Surg* 2002; **15**: 287.
14. Rabb H, Daniels F, O'Donnell M, *et al.* Pathophysiological role of T lymphocytes in renal ischemia–reperfusion injury in mice. *Am J Physiol Renal Physiol* 2000; **279**: F525.
15. Anselmo DM, Amersi FF, Shen XD, *et al.* FTY720 pretreatment reduces warm hepatic ischemia reperfusion injury through inhibition of T-lymphocyte infiltration. *Am J Transplant* 2002; **2**: 843.
16. Abe K, Yuki S, Kogure K. Strong attenuation of ischemic and postischemic brain edema in rats by a novel free radical scavenger. *Stroke* 1988; **19**: 480.
17. Houkin K, Nakayama N, Kamada K, Noujou T, Abe H, Kashiwaba T. Neuroprotective effect of the free radical scavenger MCI-186 in patients with cerebral infarction: clinical evaluation using magnetic resonance imaging and spectroscopy. *J Stroke Cerebrovasc Dis* 1998; **7**: 315.
18. Tohgi H, Kogure K, Hirai S, *et al.* Effect of a novel free radical scavenger, Edaravone (MCI-186), on acute brain infarction. *Cerebrovasc Dis* 2003; **15**: 222.
19. Nishi H, Watanabe T, Sakurai H, Yuki S, Ishibashi A. Effect of MCI-186 on brain edema in rats. *Stroke* 1989; **20**: 1236.
20. Ninomiya M, Shimada M, Harada N, Soejima Y, Suehiro T, Maehara Y. The hydroxyl radical scavenger MCI-186

protects the liver from experimental cold ischemia-reperfusion injury. *Br J Surg* 2004; **91**: 184.
21. Ninomiya M, Shimada M, Harada N, *et al.* Beneficial effect of MCI-186 on hepatic warm ischemia-reperfusion in the rat. *Transplantation* 2002; **74**: 1470.
22. Abe T, Unno M, Takeuchi H, *et al.* A new free radical scavenger, edaravone, ameliorates oxidative liver damage because of ischemia-reperfusion *in vitro* and *in vivo*. *J Gastrointest Surg* 2004; **8**: 604.
23. Okatani Y, Wakatsuki A, Enzan H, Miyahara Y. Edaravone protects against ischemia/reperfusion-induced oxidative damage to mitochondria in rat liver. *Eur J Pharmacol* 2003; **465**: 163.
24. Soeda J, Miyagawa S, Sano K, Masumoto J, Taniguchi S, Kawasaki S. Cytochrome *c* release into cytosol with subsequent caspase activation during warm ischemia in rat liver. *Am J Physiol Gastrointest Liver Physiol* 2001; **281**: G1115.
25. Kawai H, Nakai H, Suga M, Yuki S, Watanabe T, Saito KI. Effects of a novel free radical scavenger, MCI-186, on ischemic brain damage in the rat distal middle cerebral artery occlusion model. *J Pharmacol Exp Ther* 1997; **281**: 921.
26. Yanagisawa A, Miyagawa M, Ishikawa K, Murota S. Cardioprotective effect of MCI-186 (3-methyl-1-phenyl-2 pyrazolin-5-one) during acute ischemia–reperfusion injury in rats. *Int J Angiol* 1994; **3**: 12.
27. Kono H, Asakawa M, Fujii H, *et al.* Edaravone, a novel free radical scavenger, prevents liver injury and mortality in rats administered endotoxin. *J Pharmacol Exp Ther* 2003; **307**: 74.
28. Suzuki S, Toledo-Pereyra LH, Rodriguez FJ, Cejalvo D. Neutrophil infiltration as an important factor in liver ischemia and reperfusion injury. Modulating effects of FK506 and cyclosporine. *Transplantation* 1993; **55**: 1265.
29. Wiezorek JS, Brown DH, Kupperman DE, Brass CA. Rapid conversion to high xanthine oxidase activity in viable Kupffer cells during hypoxia. *J Clin Invest* 1994; **94**: 2224.
30. Yokota R, Fukai M, Shimamura T, *et al.* A novel hydroxyl radical scavenger, nicaraven, protects the liver from warm ischemia and reperfusion injury. *Surgery* 2000; **127**: 661.
31. Zhong Z, Froh M, Connor HD, *et al.* Prevention of hepatic ischemia–reperfusion injury by green tea extract. *Am J Physiol Gastrointest Liver Physiol* 2002; **283**: G957.
32. Mizoe A, Kondo S, Azuma T, *et al.* Preventive effects of superoxide dismutase derivatives modified with monosaccharides on reperfusion injury in rat liver transplantation. *J Surg Res* 1997; **73**: 160.
33. Yabe Y, Kobayashi N, Nishihashi T, *et al.* Prevention of neutrophil-mediated hepatic ischemia/reperfusion injury by superoxide dismutase and catalase derivatives. *J Pharmacol Exp Ther* 2001; **298**: 894.
34. Okatani Y, Wakatsuki A, Reiter RJ, Enzan H, Miyahara Y. Protective effect of melatonin against mitochondrial injury induced by ischemia and reperfusion of rat liver. *Eur J Pharmacol* 2003; **469**: 145.
35. Kusumoto K, Morimoto T, Minor T, Uchino J, Isselhard W. Allopurinol effects in rat liver transplantation on recovery of energy metabolism and free radical-induced damage. *Eur Surg Res* 1995; **27**: 285.
36. Schreck R, Rieber P, Baeuerle PA. Reactive oxygen intermediates as apparently widely used messengers in the activation of the NF-kappa B transcription factor and HIV-1. *EMBO J* 1991; **10**: 2247.
37. Satriano J, Schlondorff D. Activation and attenuation of transcription factor NF-κB in mouse glomerular mesangial cells in response to tumor necrosis factor-α, immunoglobulin G, and adenosine 3′:5′-cyclic monophosphate. Evidence for involvement of reactive oxygen species. *J Clin Invest* 1994; **94**: 1629.
38. Singh S, Aggarwal BB. Activation of transcription factor NF-κ B is suppressed by curcumin (diferuloylmethane). *J Biol Chem* 1995; **270**: 24995.
39. Shito M, Wakabayashi G, Ueda M, *et al.* Interleukin 1 receptor blockade reduces tumor necrosis factor production, tissue injury, and mortality after hepatic ischemia-reperfusion in the rat. *Transplantation* 1997; **63**: 143.
40. Shirasugi N, Wakabayashi G, Shimazu M, *et al.* Up-regulation of oxygen-derived free radicals by interleukin-1 in hepatic ischemia/reperfusion injury. *Transplantation* 1997; **64**: 1398.
41. Liang J, Yamaguchi Y, Matsumura F, *et al.* Calcium-channel blocker attenuates Kupffer cell production of cytokine-induced neutrophil chemoattractant following ischemia-reperfusion in rat liver. *Dig Dis Sci* 2000; **45**: 201.
42. Colletti LM, Kunkel SL, Walz A, *et al.* Chemokine expression during hepatic ischemia/reperfusion-induced lung injury in the rat. The role of epithelial neutrophil activating protein. *J Clin Invest* 1995; **95**: 134.
43. Colletti LM, Kunkel SL, Walz A, *et al.* The role of cytokine networks in the local liver injury following hepatic ischemia/reperfusion in the rat. *Hepatology* 1996; **23**: 506.
44. Yamaguchi Y, Matsumura F, Takeya M, *et al.* Monocyte chemoattractant protein-1 enhances expression of intercellular adhesion molecule-1 following ischemia-reperfusion of the liver in rats. *Hepatology* 1998; **27**: 727.
45. Martinez-Mier G, Toledo-Pereyra LH, Ward PA. Adhesion molecules in liver ischemia and reperfusion. *J Surg Res* 2000; **94**: 185.

STEM CELLS®
Original Article

Crucial Roles of Mesodermal Cell Lineages in a Murine Embryonic Stem Cell–Derived In Vitro Liver Organogenesis System

SHINICHIRO OGAWA,[a,b] YOH-ICHI TAGAWA,[a] AKIKO KAMIYOSHI,[a] AKIHIRO SUZUKI,[a] JUN NAKAYAMA,[c] YASUHIKO HASHIKURA,[b] SHINICHI MIYAGAWA[b]

[a]Division of Laboratory Animal Research, Research Center for Human and Environmental Sciences, Shinshu University;
[b]Department of Surgery, Shinshu University School of Medicine;
[c]Department of Pathology, Shinshu University School of Medicine, Shinshu, Japan

Key Words. Embryonic stem cell • Liver • Organogenesis • Cardiomyocyte • Endothelial cell • In vitro system

ABSTRACT

Recent studies in the field of regenerative medicine have exploited the pluripotency of embryonic stem (ES) cells to generate a variety of cell lineages. However, the target has always been only a single lineage, which was isolated from other differentiated cell populations. In the present study, we selected sublines with a high capability for differentiation to contracting cardiomyocytes and also produced germline chimeric mice from a parent ES line. We also succeed in establishing embryoid bodies prepared from the ES cells that differentiated into not only hepatocytes but also at least two mesodermal lineages: cardiomyocytes that supported liver development and endothelial cells corresponding to sinusoids. This allowed the development of an in vitro system using murine ES cells that approximated the events of liver development in vivo. The expression of *albumin* was significantly higher in cardiomyocytes that had arisen in differentiated ES cells than in those that had not. Our in vitro system for liver organogenesis consists of a blood/sinusoid vascular-like network and hepatocyte layers and shows higher levels of hepatic function, such as albumin production and ammonia degradation, than hepatic cell lines and primary cultures of murine adult hepatocytes. This innovative system will lead to the development of second-generation regenerative medicine techniques using ES cells and is expected to be useful for the development of bioartificial liver systems and drug-metabolism assays. STEM CELLS *2005;23:903–913*

INTRODUCTION

The liver develops from the ventral foregut in vertebrates, receiving multiple stimuli in the form of growth factors, cytokines, and hormonal factors, as well as intercellular and matrix cellular interactions [1–5]. In particular, the precardiac mesoderm produces factors that trigger hepatic development [6, 7], that is, cardiomyocytes support liver organogenesis (Fig. 7A). The signaling of fibroblast growth factor (FGF), produced in the cardiac mesoderm, induces the initial step of hepatogenesis in the ventral endoderm at E8.5–9.5 of mouse development, resulting in the activation of albumin and α-fetoprotein expressions [4, 6, 8]. As the hepatic precursor cells migrate into the septum transversum to form a liver bud [9], endothelial progenitor cells arise there simultaneously in close association with early developing hepatoblasts and hepatogenesis [10]. These endothelial cells develop a fenestrated morphology to form the hepatic sinusoids [11–13], and then finally the liver is completed, with its multiple and specific functions.

In the field of regenerative medicine, the pluripotency of embryonic stem (ES) cells has been applied to obtain a vari-

Correspondence: Yoh-ichi Tagawa, Ph.D., Department of Biomolecular Engineering, Graduate School of Bioscience and Biotechnology, Tokyo Institute of Technology, B-51 4259 Nagatsuta-cho, Midori-ku, Yokohama, Kanagawa, 226-8501 Japan. Telephone: 81-45-924-5791; Fax: 81-45-924-5815; e-mail: ytagawa@bio.titech.ac.jp Received October 23, 2004; accepted for publication March 20, 2005.
 1066-5099/2005/$12.00/0 doi: 10.1634/stemcells.2004-0295

ety of cell lineages. However, the targets of these systems have always been limited to only a single lineage, which was isolated from other differentiated cell populations. There have been a few reports on the differentiation of murine ES cells to hepatocyte-like or albumin-producing cells [14–19]. However, these studies focused only on hepatocytes as a single-cell lineage and did not refer to liver organogenesis. It also has been reported that hepatocyte-like cells spontaneously differentiate from human ES cells [20], as well as previous studies using murine ES cells. In particular, there has been no description about the roles of cardiomyocytes and endothelial cells in hepatocyte differentiation, although one previous study has detected albumin-positive cells adjacent to cardiomyocytes in teratoma-derived human ES cells in severe combined immunodeficiency mice [20]. Cardiac mesoderm has a strong capacity to induce liver organogenesis [4, 6, 8]. These cell lineages can also be obtained from ES cells. Therefore, we considered that emergence of cardiomyocytes would be necessary for liver morphogenesis from ES cells in vitro. Our purpose in the present study was to establish a system for in vitro hepatic morphogenesis consisting of not only hepatocytes but also cell lineages supporting hepatic differentiation, such as cardiomyocytes and endothelial cells, which correspond to those involved in liver organogenesis in vivo, from murine ES cells. We exploited the pluripotency of ES cells for differentiation of these cell lineages, which included hepatocytes, cardiomyocytes, and endothelial cells, and succeeded in establishing a novel system of hepatic morphogenesis from murine ES cells based on naturally occurring embryological events, that is, with contributions from cardiac mesoderm and endothelial cell lineages.

Materials and Methods

Cell Culture

E14-1 ES cells derived from 129/Ola were grown on mitomycin C–treated mouse embryonic fibroblast feeder layers to maintain them in an undifferentiated state in Dulbecco's modified Eagle's medium (DMEM) (Invitrogen, Tokyo, http://www.invitrogen.com) containing 20% fetal bovine serum (FBS) (Hyclone, Logan, UT, http://www.hyclone.com), 1 mM sodium pyruvate (Invitrogen), 100 μM nonessential amino acids (Invitrogen), 100 μM 2-mercaptoethanol (Sigma, St. Louis, http://www.sigmaaldrich.com), and 10^3 U/ml leukemia inhibitory factor (LIF) (Chemicon, CA, http://www.chemicon.com). The cells were dissociated with 0.25% trypsin, 1% chicken serum (Invitrogen), and 1 mM EDTA in phosphate-buffered saline (PBS) and resuspended in Iscove's modified Dulbecco's medium (IMDM) (Invitrogen) containing 20% FBS, 1 mM sodium pyruvate, 100 μM nonessential amino acids, and 100 μM 2-mercaptoethanol without LIF and then formed into a hanging drop at a concentration of 1,000 cells per 50-μl drop. The hanging drop was cultured in an atmosphere of 5% CO_2 at 37°C for 5 days. An individual 5-day-old embryoid body (EB) was plated in each well of a gelatin-coated 96-well plate, and the growth factor was added to the culture medium. The day when the 5-day-old EBs were plated in the dish was denoted day 0 (A0). Human recombinant acidic fibroblast growth factor (aFGF) (Invitrogen) was added to the differentiation medium at a concentration of 100 ng/ml 2 days after plating of the 5-day-old EBs (A2), and 20 ng/ml human recombinant hepatocyte growth factor (HGF) (Genzyme/Techne, Minneapolis, http://www.g-tonline.com) was added at A4. Then, at A6, 10 ng/ml mouse recombinant oncostatin M (Genzyme/Techne), 100 nM dexamethasone (MP Biomedicals, Irvine, CA, http://www.mpbio.com), ITS (insulin 10 μg/ml, transferrin 5 μg/ml, selenium 5 ng/ml; Invitrogen), and 10 mM nicotinamide (Nakalai tesque, Kyoto, Japan, http://www.nacalai.co.jp) were added. The emergence frequency of contracting cells in the EB outgrowths, indicating cardiac muscle differentiation, was monitored daily. Emergence frequency was expressed as a percentage, where 100% meant detection of a contractile area in all wells containing EB outgrowths. Twenty recloned 5-day-old EBs were plated on a 6-cm dish coated with gelatin as a semi–large-scale culture.

To obtain fetal hepatocytes, mouse liver at E15 was minced and dissociated with collagenase II (Sigma) in Hanks' buffer (Invitrogen). The cells were seeded on a gelatin-coated dish in DMEM supplemented with 10% FBS, 100 μM nonessential amino acids, and 100 U/ml penicillin-100 μg/ml streptomycin-292 μg/ml glutamine for a few hours and washed once with the same medium. The medium was replaced every day.

Primary adult hepatocytes were isolated from male 129/SvJ mice by the two-step collagenase perfusion method. The hepatocytes were separated from the resulting cell suspension by centrifugation and then by centrifugation through a 50% Percoll (Sigma) gradient. Isolated hepatocytes were plated onto gelatin-coated dishes.

Production of Chimeric Mice

Chimeric mice were produced by the modified aggregation method [21]. This involved aggregation of 10 to 15 ES cells with two (BDF1 × C57BL) F_1 eight-cell-stage embryos, from which the zona pellucida had been removed with Tyrode's solution (Sigma), were placed in a hole on a plastic dish and cultured overnight. The ES cells and eight-cell-stage embryos became a single blastocyst, and the blastocysts were then transferred to the uterus of pseudopregnant female ICR mice. Male chimeric mice were then bred with C57BL/6 female mice, and germ-line transmission of the ES cells was checked by the agouti coat color of the offspring.

RNA Extraction and Reverse Transcription–Polymerase Chain Reaction Analysis

Total RNA was extracted from the outgrowths of the EBs using a MagEXtractor mRNA kit (Toyobo, Tokyo, http://www.toyobo.co.jp/e). Briefly, 2-μg aliquots of total RNA were reverse tran-

scribed to cDNAs using a Superscript II first-strand synthesis system with an oligo dT primer (Invitrogen). Semiquantitative reverse transcription–polymerase chain reaction (RT-PCR) was performed using Ex Taq DNA polymerase (Takara, Tokyo, http://www.takara-bio.com) with the following primer sets. For each experiment, a housekeeping gene, hypoxanthine phosphoribosyltransferase, was amplified with 25 cycles to normalize the expressions of other genes in the sample. The forward and reverse primers were located at different exons to discriminate the product from the targeted mRNA or its genomic DNA. The PCR primers used were as follows: albumin, GCTACGGCACAGTGCTTG and CAGGATTGCAGACAGATAGTC (product size, 265 bp; annealing temperature, 65°C); α-fetoprotein, TCGTATTCCAACAGGAGG and AGGCTTTTGCTTCACCAG (product size, 173 bp; annealing temperature, 65°C); transthyretin, CTCACCACAGATGAGAAG and GGCTGAGTCTCTCAATTC (product size, 223 bp; annealing temperature, 56°C); α1–anti-trypsin, AATGGAAGAAGCCATTCGAT and AAGACTGTAGCTGCTGCAGC (product size, 483 bp; annealing temperature, 50°C); Oct3/4, AGCACGAGTGGAAAGCACT and CTCATTGTTGTCGGCTTCCT (product size, 339 bp; annealing temperature, 60°C); tyrosine aminotransferase, ACCTTCAATCCCATCCGA and TCCCGACTGGATAGGTAG (product size, 205 bp; annealing temperature, 66°C); tryptophan 2,3-deoxygenase, TGCGCAAGAACTTCAGAGTGA and TGCGCAAGAACTTCAGAGTGA (product size, 419 bp; annealing temperature, 62°C); liver-specific organic anion transporter-1, TGCGCAAGAACTTCAGAGTGA and TGAGTTGGACCCCTTTTCAC (product size, 226 bp; annealing temperature, 65°C); asialoglycoprotein receptor-1, GCTGGAAAAACAGCAGAAGG and CTGTTCCATCCACCCATTTC (product size, 358 bp; annealing temperature, 65°C); asialoglycoprotein receptor-2, CGGACCCTGAAAGAAACCTT and ATGAAACTGGCTCCTGTGCT (product size, 410 bp; annealing temperature, 66°C); HGF, AGACACCACACCGGCACAGT and ATAGGGCAATAATCCCAAGG (product size, 484 bp; annealing temperature, 65°C); FGF-1, ACCGAGAGGTTCAACCTGCC and GCCATAGTGAGTCCGAGGACC (product size, 386 bp; annealing temperature, 66°C); vascular endothelial growth factor (VEGF), CAGGCTGCTGTAACGATGAA and AATGCTTTCTCCGCTCTGAA (product size, 206 bp; annealing temperature, 65°C); VEGFR1, TGTGGAGAAACTTGGTGACCT and TGGAGAACAGCAGGACTCCTT (product size, 504 bp; annealing temperature, 65°C); VEGFR2, TCTGTGGTTCTGCGTGGAGA and GTATCATTTCCAACCACCC (product size, 269 bp; annealing temperature, 55°C); platelet-endothelial cell adhesion molecule-1 (PECAM-1), GTCATGGCCATGGTCGAGTA and AGCAGGACAGGTCCAACAAC (product size, 168 bp; annealing temperature, 65°C); atrial natriuretic peptide, ATGGGCTCCTTCTCCCATCAC and TGTTGCAGCCTAGTCCACTC (product size, 541 bp; annealing temperature, 65°C); and hypoxanthine phosphoribosyltransferase, GTTGGATACAGGCCAGACTTTGTTG and GAGGGTAGGCTGGCCTATAGGCT (product size, 269 bp; annealing temperature, 65°C).

Immunohistochemical Analysis

Twenty EBs were cultured on gelatin-coated glass coverslips in a six-well plate. EB outgrowths on the coverslips were fixed with 4% paraformaldehyde/PBS for 20 minutes and then permeabilized with 0.1% Triton X for 10 minutes at room temperature. The fixed samples were incubated in blocking buffer containing 4% donkey serum (Jackson Immunoresearch, Baltimore, http://www.jacksonimmuno.com) for 10 minutes at room temperature. They were then incubated with the primary antibody overnight at 4°C and with the secondary antibody for 1 hour in a humidified chamber. The following antibodies were used: rabbit immunoglobulin (IgG) against mouse albumin (1:250; MP Biomedicals), goat IgG against mouse PECAM-1 (1:250; Santa Cruz Biotech, CA, http://www.scbt.com), tetramethylrhodamine isothiocyanate–conjugated swine anti-rabbit immunoglobulin (1:60; DakoCytomation A/S, Glostrup, Denmark, http://www.dakocytomation.com), and fluorescein-conjugated donkey anti-goat IgG (1:100; Jackson Immunoresearch, West Grove, PA). For nuclear staining, the cells were incubated for 5 minutes at room temperature with DAPI (4,6 diamidino-2-phenylindole). The samples were mounted in DakoCytomation fluorescent mounting medium and observed using a fluorescence microscope (BX 60; Olympus, Tokyo, http://www.olympus-global.com/en/global) and a confocal laser microscope (TCS SP2; Leica, Manheim, Germany, http://www.leica.com/index.html).

Western Blotting Analysis

ES cells and EBs were homogenized in buffer containing 20 mM Tris-HCl, pH 7.5, 150 mM NaCl, 1% Nonidet P-40, 0.1% SDS, 1% sodium deoxycholate, 2 mM EDTA, 1 mM phenylmethylsulfonyl fluoride, 2 μg/ml aprotinin, 10 μg/ml leupeptin, and 5 μg/ml pepstatin, centrifuged at 12,000 rpm for 10 minutes at 4°C, and the supernatants were collected. Protein concentration was measured with a bicinchoninic acid protein assay (BCA protein assay kit; Pierce, Rockford, IL, http://www.piercenet.com). The same amounts (10 μg each lane) of proteins from cell homogenates were electrophoresed on 8% polyacrylamide gels. Proteins were transferred onto polyvinylidene difluoride membranes by electro blotting. The membranes were blocked for 1 hour at room temperature with 5% nonfat dried milk and 0.1% bovine serum albumin in tris-buffered saline (TBS) containing 0.1% (vol/vol) Tween 20 (TBS-T) and incubated for 1 hour with peroxidase-conjugated sheep anti-rabbit antibody (GE Healthcare, Piscataway, NJ, http://www.gehealthcare.com) diluted in TBS-T containing 5% FBS. After washing with TBS-T, the blots

were developed by enhanced chemiluminescence (GE Healthcare) and exposed to x-ray film (RX-U; Fuji, Kawasaki, Japan, http://home.fujifilm.com).

Treatment with Thalidomide or CBO-P11

Thalidomide (N-[2,6-dioxo-3-piperidinyl] phthalimide; Tocris Cookson, Ellisville, MO, http://www.tocris.com) was dissolved in dimethyl sulfoxide and added to the medium at the indicated concentration. CBO-P11 (cyclo-VEGI) (DFPQIMRIKPHQGQHIGE) (Calbiochem, San Diego, http://www.emdbiosciences.com/html/CBC/home.html), a cyclopeptidic vascular endothelial growth inhibitor, was dissolved in water and added to the medium at a concentration of 10 μM. These chemicals were added to the medium after 20 five-day-old EBs had been plated on the dish (A0). The medium was replaced every day.

Ammonia Modification Function Assay

To examine cellular ammonia degradation activity, 2 mM NH_4Cl was added to the serum-free culture medium of 30 or 50 EBs at days 10 and 18 after plating and further incubated for 24 hours. The concentration of NH_4Cl remaining in the medium was measured at various time points by a modified indophenol method using a commercial kit (Ammonia-test Wako; Wako, Osaka, Japan, http://www.wako-chem.co.jp).

Results

Roles of Embryonic Stem Cell–Derived Cardiomyocytes in Hepatic Differentiation from Murine Embryonic Stem Cells

As is the case in in vivo development, the emergence of cardiomyocytes is necessary for liver organogenesis in an in vitro differentiation system using ES cells. As an initial approach for inducing murine ES cells to undergo hepatic morphogenesis, we established a system for spontaneous differentiation to contracting cardiomyocytes with a high frequency of emergence. A single 5-day-old EB comprised of dissociated murine ES cells was plated onto gelatin-coated plates and allowed to adhere to the bottom of the plate. The EB outgrowths began to contract spontaneously within 5 days after plating. These ES cell–derived contracting cells were considered to be cardiomyocytes based on specific gene expression (Fig. 1B) and pharmacological responses. The outgrowths of EBs were cultured in the differentiation medium for 18 days (A18) after adhesion to the well bottom. The expression of *albumin* was compared in groups of EBs in which cardiomyocytes had and had not arisen at A10; the levels of albumin expression were significantly higher in those with outgrowths of contracting cardiomyocytes than in those without (Fig. 1B), suggesting that the ability to differentiate to cardiomyocytes in the ES cell population and the emergence of cardiomyocytes in the EB outgrowths are important for endodermal and hepatocyte differentiation.

To increase the efficiency of liver organogenesis from ES cells, it was considered important to increase the frequency of cardiomyocyte emergence in the EB outgrowths. The frequency of cardiomyocyte emergence at Ab-3 was less than 30% using the parental line of the E14-1 ES cells at passages 14 through 18, whereas the frequency was almost 100% using some sublines (My-1 and Ab-3) other than My-5, which were recloned from the parental line E14-1 (Fig. 1A). Ability for the production of chimeric mice was also compared in the parental line and these E14-1 sublines. The chimera-forming ability of the parental E14-1 was 2 germ-line/17 chimeric mice from

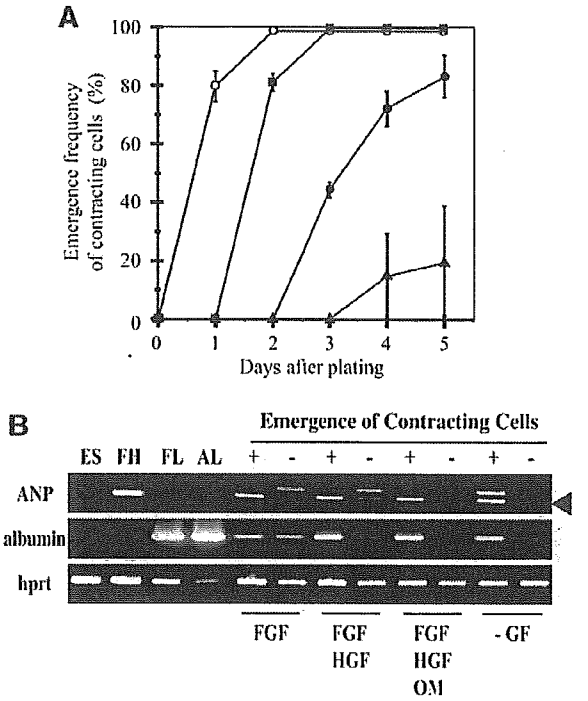

Figure 1. Establishment of a system for allowing differentiation of ES cells to cardiomyocytes at a frequency of almost 100% for hepatic differentiation. **(A):** Comparison of the time courses of the frequency of emergence contractile cells from outgrowths of EBs prepared from the parental line of E14-1 ES cells (●), subline My-1 (○), Ab-3 (■), and My-5 (▲). **(B):** Expression of albumin as a representative hepatic marker and of ANP as an atrial marker was determined by reverse transcription–PCR during differentiation of EBs. PCR amplication of ANP and albumin was carried out for 30 cycles. Human recombinant aFGF was added to the differentiation medium at a concentration of 100 ng/ml 2 days after plating of the 5-day-old EBs on the dish (A2), and then 20 ng/ml human recombinant HGF was added at A4. Then with 10 ng/ml mouse recombinant OSM, 100 nM dexamethasone, ITS (insulin 10 μg/ml, transferrin 5 μg/ml, selenium 5 ng/ml), and 10 mM nicotinamide (Nacalai) were added at A6. Arrowhead indicates the expected band of ANP. Abbreviations: aFGF, acidic fibroblast growth factor; AL, mouse adult liver; ANP, atrial natriuretic peptide; EB, embryoid body; ES, embryonic stem; GF, growth factor; FH, mouse fetal heart at E15; FL, mouse fetal liver at E15; HGF, hepatocyte growth factor; OSM, oncostatin M; PCR, polymerase chain reaction.

171 ES-aggregated embryos, whereas that of a subline Ab-3 was 4 germ-line/18 chimeric mice from 155 ES-aggregated embryos. It is very important that undifferentiated and pluripotent ES cells should be present in these cultures for differentiation not only to cardiomyocytes but also to albumin-producing hepatocytes and endothelial cells corresponding to the developmental stages of the liver. For the following experiments, we used the selected subline, Ab-3, which showed high capability for differentiation to cardiomyocytes and also for production of germ-line chimeric mice, within six passages.

Expression and Function of Liver-Specific Gene Expressions and Functions in Murine Embryonic Stem Cell–Derived Hepatic Morphogenesis

Twenty 5-day-old EBs were placed together on gelatin-coated dishes in differentiation medium as a semi–large-scale system, because the absolute numbers of cells would be needed for hepatic development. Contracting cardiomyocytes emerged in the central area of EB outgrowth. A heterologous population was considered important for in vitro hepatic morphogenesis using murine ES cells. The expressions of endodermal/hepatocyte-specific genes, such as transthyretin, α-fetoprotein, α1-antitrypsin, and albumin, at the various stages of EB differentiation were examined (Fig. 2A). The levels of expression of these genes increased markedly as differentiation of the EBs proceeded, whereas that of *Oct-3/4*, a marker of undifferentiated ES cells, decreased. The levels of expression of liver-specific genes and *Oct-3/4* in the presence of growth factor were the same as those in the absence of growth factor, suggesting that cardiomyocytes were not induced in the presence of growth factor. We also confirmed that albumin protein was detectable in the differentiated outgrowths of EBs at A4 and increased gradually throughout differentiation (Fig. 2B), corresponding to the changes in mRNA levels (Fig. 2A).

As a second approach for inducing hepatic morphogenesis from ES cells, aFGF, HGF, and oncostatin M were added to the cultures to investigate the effects of growth factors. The levels of expression of albumin, tyrosine aminotransferase (*TAT*), and tryptophan oxygenase (*TO*) were significantly higher in the presence than in the absence of additional growth factors at A10, corresponding to the early differentiation stage of EBs. This suggests that the addition of growth factors artificially induces the expression of mature hepatocyte-specific genes or accelerates differentiation in the system at an early stage (Fig. 2C). On the other hand, at A18, corresponding to the late differentiation stage, the levels of expression of albumin, *TAT*, *TO*, and asialo glycoprotein receptors (*ASGR1, ASGR2*) in the EB were almost the same levels under conditions with and without

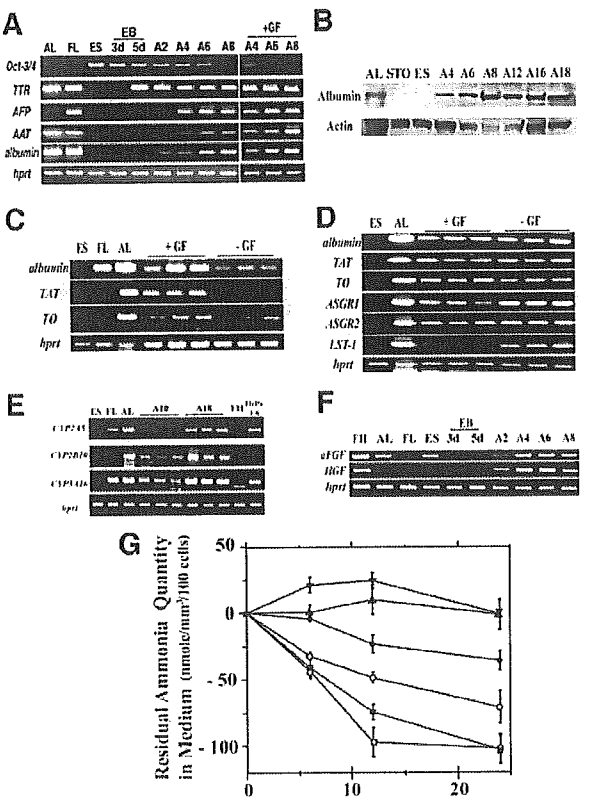

Figure 2. Expression by ES cell–derived hepatocytes of a variety of liver-specific genes, production of albumin protein, and ammonia modification function. **(A):** The expression of endodermal-specific genes was examined in the outgrowths of EBs from before plating (3- and 5-day-old EBs) to 8 days after plating (A8) by RT-PCR. PCR amplification of *Oct-3/4, TTR, AFP, AAT,* and *albumin* was carried out for 30 cycles. Five-day-old EBs were plated on gelatin-coated dishes and cultured in the absence of any growth factors. **(B):** The level of albumin protein was quantified by Western blotting analysis during hepatic differentiation of EBs. EBs were cultured in the absence of any growth factors for 18 days. **(C, D):** Expression of albumin and mature hepatocyte-specific genes expression was detected in the EB outgrowths at A10 **(C)** and A18 **(D)**. Comparison of cultures in the presence or absence of additional growth factors. PCR amplification of *albumin* was carried out for 25 cycles. Amplification of TAT, ASGR-1, ASGR-2, and LST-1 was carried out for 40 cycles. Amplification of TO was carried out for 30 cycles. **(E):** Expression of CYP family genes, such as Cyp2A5, 2B10, and 3A16, was detected by RT-PCR (40 cycles, respectively) in the EB outgrowths at A10 and A18 cultured in the absence of additional growth factors. **(G):** Ammonia modification function was measured in EB outgrowths at A18. The amounts of residual ammonia in 100 cells are indicated, which were calculated from the quantity of prepared genomic DNA. □, primary adult mouse hepatocyte culture; ■, outgrowth of 50 EBs at A18; ○, 30 EBs at A18; ●, 30 EBs at A10; ▼, mouse hepatoma cell line, HePa1–6; ▲, ES E14-1. **(F):** Endogenous aFGF and HGF gene expression was detected by RT-PCR (40 cycles, respectively) in the EB outgrowths during differentiation in the absence of these additional growth factors by RT-PCR. Arrowhead indicates the expected band of ANP. Abbreviations: aFGF, acidic fibroblast growth factor; AL, mouse adult liver; EB, embryoid body; ES, embryonic stem; GF, growth factor; FL, mouse fetal liver at E15; HGF, hepatocyte growth factor; RT-PCR, reverse transcription–polymerase chain reaction; TAT, tyrosine aminotransferase.

additional growth factors. Furthermore, *liver-specific transporter (LST-1)* mRNA was detected only in the absence of any growth factor (Fig. 2D), suggesting that these additional factors were not essential for hepatic differentiation and maturation from ES cells in our system. The expressions of some CYP genes were also detectable under conditions without growth factors (Fig. 2E).

To investigate whether the outgrowths of EBs could supply these growth factors themselves, the expressions of these genes were analyzed in EBs without these growth factors. Endogenous *aFGF* and *HGF* expression was detected in the outgrowths in the absence of the additional growth factors (Fig. 2F), suggesting that addition of these growth factors is not necessary for hepatic differentiation of EBs, as they are produced endogenously.

Assay of ammonia degradation, a representative hepatic function, was also carried out. Interestingly, the level of ammonia degradation was markedly higher in the differentiated EB outgrowths than in the hepatocyte cell line, HePa1-6, and in primary cultures of murine hepatocytes (Fig. 2E).

To investigate the distribution of albumin-positive cells in the EB outgrowths at A10 and A18, we performed immunohistochemical analyses using anti-mouse albumin antibody. The albumin-positive cells were visualized adjacent to the contracting cardiomyocytes, around the central area of the outgrowths, at A10 (Fig. 3A). These albumin-positive cells formed clusters and showed an islet-like morphology in the outgrowths (Figs. 3A, 3B). At A18, corresponding to the late stage of hepatic differentiation, these colonies had grown and were strongly detected, as can be seen in Figure 3C, suggesting that these cells were proliferating and expanding.

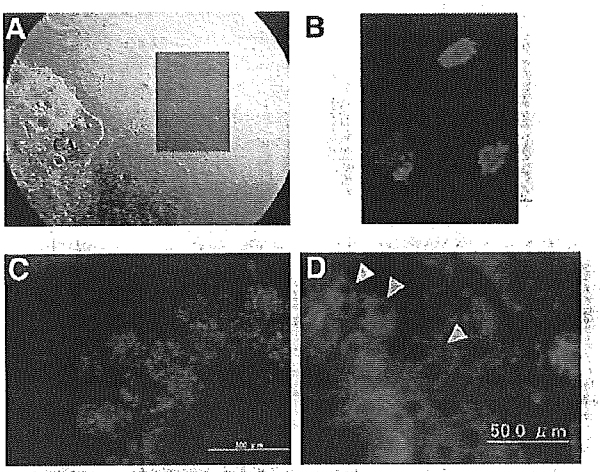

Figure 3. Albumin-positive cells observed as expanding colonies in the outgrowths of EBs. **(A):** Photomicrograph showing the contracting region and albumin-positive areas in the outgrowths of differentiated EBs at A10 in the absence of any growth factors. The shaded square is magnified in **(B)**. **(B–D):** Immunohistochemical analysis of the EB outgrowths at **(B)** A10 and **(C, D)** A18 using anti-albumin (red). White arrowheads indicate the binuclear cells in the outgrowths of the EB. These cultures were also carried out in the absence of any growth factors. Abbreviations: CA, contracting cardiomyocyte area; EB, embryoid body.

Morphology of Murine Embryonic Stem Cell–Derived Hepatocytes

Murine hepatocytes contained two morphologically distinct populations, a mononuclear population and a binuclear population. Hepatocytes in the resting liver consist predominantly of binuclear hepatocytes, whereas those in the regenerating liver are mainly mononuclear hepatocytes [22]. Some of these albumin-positive cells were binuclear, which is a characteristic of mature hepatocytes in mice (Fig. 3D). Thus, these cells were confirmed to be murine hepatocytes on the basis of morphology as well as by hepatic function and gene expression analysis. In addition to hepatic function and expression in our cultures, morphological evidence also suggested that the albumin-producing cells derived from ES cells in our system were hepatocytes.

Vasculogenesis in the System to Induce Murine Embryonic Stem Cells to Hepatic Morphogenesis

The contribution of the nonparenchymal hepatic cell population is necessary for hepatic in vitro morphogenesis from ES cells. Expression of *VEGF, VEGFR1,* and *VEGFR2* was detected from the EB in the period from before plating to the late stage of differentiated EB, and *CD31/PECAM-1,* a definitive endothelial cell–specific marker, began to be expressed at the stage of EB formation and continued to be detectable until the late stage of differentiation of the EB outgrowths (Fig. 4A), suggesting that vasculogenesis had been activated in this system. Indeed, CD31/PECAM-1–positive cells were shown to form network structures (Fig. 4C), indicating that CD31/PECAM-1–positive cells organized the formation of vascular networks in the EB outgrowths. In the presence of additional growth factors, few CD31/PECAM-1–positive cells were seen to be organizing capillary networks, which were twisted and slender (Fig. 4D), compared with those in the absence of additional growth factors.

To analyze the interactions between albumin-producing cells and these endothelial cells, the EB outgrowths at both the early and late stages after plating were stained with anti-albumin and anti-CD31/PECAM-1 antibodies. Using these antibodies discriminated parenchymal or nonparenchymal cells as anti-albumin–positive or anti-CD31/PECAM-1–positive cells, respectively, in mixed control cultures of cells prepared from mouse liver (Fig. 4B). Interestingly, the CD31/PECAM-1–positive cells were seen to be migrating in the albumin-positive areas of the EB outgrowths at A10 and made contact with the juxtapositions of the albumin-positive cells (Fig. 4E), similar to the situation liver organogenesis in the developing embryo [10]. As can be seen in Figures 4E and 4F, albumin-positive cells were proliferating from A10 to A18. The CD31/PECAM-1–positive cells were seen to be

proliferating and organizing networks with the spread of the albumin-positive area in the EB outgrowths at A18 (Fig. 4F), suggesting that these endothelial cells had a marked influence on formation of hepatic tissue within EBs.

To obtain conclusive evidence that vasculogenesis was necessary for hepatocytes to arise and grow in the EB outgrowth, vasculogenesis was inhibited by addition of thalidomide to the differentiation medium. First, the emergence frequency of contracting cardiomyocytes was significantly lower with the addition of thalidomide (26.7% ± 12.0% at 25 mg/L, 6.8% ± 4.2% at 100 mg/L) at A3 than without thalidomide (99.5% ± 0.5%), suggesting that thalidomide was able to inhibit the differentiation of ES cells to cardiomyocytes. The results of confocal microscopy analysis (Figs. 5A–5C) indicated that thalidomide could strongly inhibit the differentiation of CD31/PECAM-1–positive cells in the EB outgrowths compared with the control cultures without thalidomide. In addition, the albumin-positive area was significantly smaller in differentiated EB outgrowths exposed to thalidomide at A18 compared with the control culture in the absence of thalidomide (Fig. 5A), and the density and area of the vascular-like network consisting of ES-derived CD31/PECAM-1–positive endothelial cells were much lower in the thalidomide-treated EB outgrowths than in the absence of thalidomide. The expression of *VEGFR1*, *VEGFR2*, and *PECAM-1* was inhibited by thalidomide in a dose-dependent manner. These results of immunohistochem-

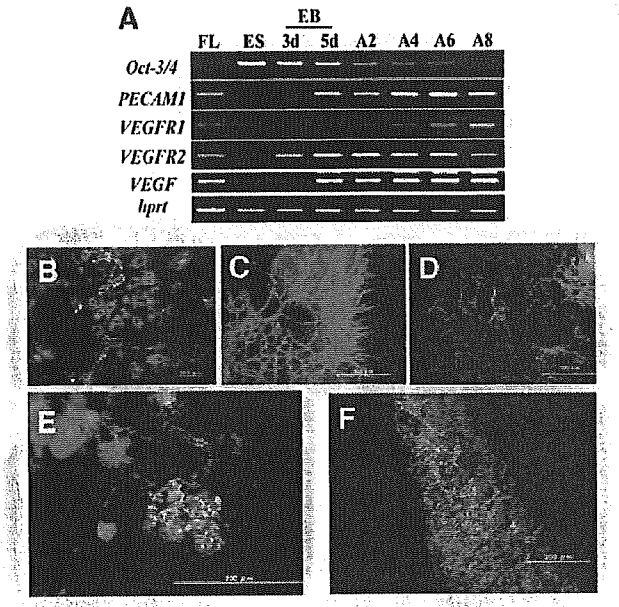

Figure 4. Hepatic morphogenesis derived from outgrowths of EBs consisting of albumin-positive hepatocytes and CD31/PECAM-1–positive endothelial cells expanding into vessel-network structures. **(A):** Endothelial development-associated gene expression was detected by reverse transcription–polymerase chain reaction analysis and activated during the differentiation of EBs. **(B):** Immunohistochemical analysis, with anti-albumin (red) and anti-CD31/PECAM-1 (green) antibodies, in mixed cultures of embryonic liver cells in vitro as a control. **(C, D):** CD31/PECAM-1–positive cells were shown to form a network structure in the presence of growth factors **(D)** and in the absence of growth factors **(C)**. The outgrowths of EBs at A18 were stained with CD31/PECAM-1 antibodies. Without exogenous growth factors, a part of the outgrowth EBs was shown as vessel-like formation. **(E, F):** Immunohistochemical analysis of the EB outgrowth at A10 **(E)** and A18 **(F)** using anti-albumin (red) and anti-CD31/PECAM-1 (green) antibodies in the absence of any growth factors. Abbreviations: EB, embryoid body; ES, embryonic stem; FL, mouse fetal liver at E15; PECAM-1, platelet-endothelial cell adhesion molecule-1; VEGFR, vascular endothelial growth factor receptor.

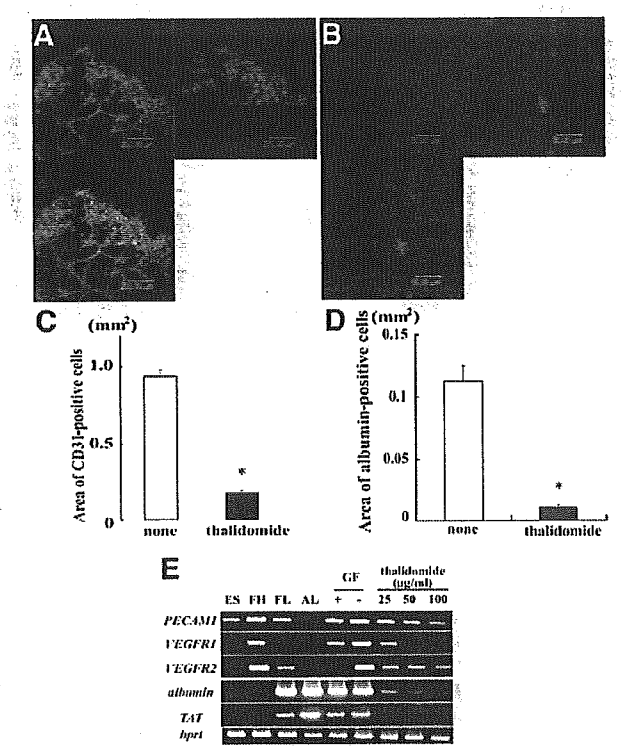

Figure 5. Dependence of hepatic morphogenesis depends on angiogenesis or vasculogenesis in the differentiated EBs. **(A, B):** Immunohistochemical analysis of the EB outgrowths at A18 using anti-CD31/PECAM-1 antibody in the presence of 100 μg/ml thalidomide for 18 days **(B)** and without thalidomide as a control **(A)**. **(C, D):** Quantitative analysis of the CD31/PECAM-1–positive area in the EB outgrowths at A18 was performed using the Scion image Beta 4.0.2 software in each of 15 selected individual fields from three independent experiments. Data are given as mean values ± standard error. Student's *t*-test for unpaired data was applied as appropriate. Difference of $p < .001$ was considered significant. **(E):** Endothelial cell and hepatocyte-associated gene expression was analyzed by reverse transcription–PCR in the thalidomide-treated EB outgrowths of the EBs at A18. PCR amplification of *PECAM-1*, *VEGFR1*, *VEGFR2*, and *TAT* was carried out for 40 cycles. Amplification of *albumin* was carried out for 30 cycles. Abbreviations: AL, mouse adult liver; ES, undifferentiated ES cells; FH, mouse fetal heart at E15; FL, mouse fetal liver at E15; GF, growth factor; PCR, polymerase chain reaction; PECAM-1, platelet-endothelial cell adhesion molecule-1; TAT, tyrosine aminotransferase; VEGFR, vascular endothelial growth factor receptor.

ical and RT-PCR analyses suggested that differentiation to endothelial cells was strongly inhibited by thalidomide. Expression of *albumin* and *TAT* was detected in the EBs at A18 in the absence, but not in the presence, of thalidomide (Fig. 5F).

Furthermore, to address the potential role of endothelial cell differentiation and proliferation in the growth of hepatocytes from ES cells, CBO-P11, a VEGF receptor–specific inhibitor, was added in this system. CD31/PECAM-1–positive cells were reduced by addition of CBO-P11 in the EB outgrowths at A18 compared with the control (Figs. 6A–6C). In the presence of CBO-P11, the morphology of the small CD31/PECAM-1–positive area was truncated and disconnected (Fig. 6B). Corresponding to the CD31/PECAM-1–positive cell populations, no albumin-positive cells were observed in the CBO-P11–treated EB outgrowths, whereas there were many albumin-positive cells in the control (Figs. 6A, 6B, 6D). The expression of *PECAM-1* was significantly lower in the CBO-P11–treated EB outgrowths than in the control without CBO-P11. Interestingly, no expression of albumin or TAT was detected in the EBs at A18 in the presence of CBO-P11 (Fig. 6F). The results of these experiments involving treatment with thalidomide and CBO-P11 suggest that CD31/PECAM-1–positive cells have a crucial role in the hepatic differentiation of ES cells.

Discussion

The purpose of this study was to devise an in vitro system that would allow liver morphogenesis from ES cells, reproducing the events of liver development in vivo. We first considered it necessary to promote the differentiation of outgrowths from EBs, derived from dissociated ES cells, to cardiomyocytes at high efficiency. Selected sublines from the parental ES cells showed a high frequency of emergence of cardiomyocytes and albumin-positive cells, whereas the frequency of cardiomyocyte emergence from the parental ES cells was not so high because of the heterogeneity of the ES cell culture in which albumin-positive cells failed to appear. The same effect was observed in our culture system, suggesting that the initial pluripotency of ES cells contributed to the differentiation of EBs to beating cardiomyocytes, and after induction to mesodermal lineages hepatic differentiation and maturation occurred in the EB outgrowths. Naggy et al. [23] described that recloned ES cell sublines could contribute significantly to the production of chimeric mice and for germ-line transmission in these mice compared with the parental line and could also become a complete body using ES cell–tetraploid aggregation [23, 24], because after a high number of passages, an ES cell culture is a heterogeneous mixture of undifferentiated and differentiated populations. It is very important for undifferentiated and pluripotent ES cells to be present in these cultures for differentiation not only to cardiomyocytes but also to albumin-producing hepatocytes and endothelial cells, corresponding to the various developmental stages of the liver. We tested several sublines of ES cells for their efficiency in the production of chimeric mice that would have the potential for germ-line transmission and a high frequency of cardiomyocyte emergence. It is interesting that the ES cell sublines that transmitted the germ line in chimeric mice at high efficiency corresponded to those with a frequency of cardiomyocyte emergence of almost 100%. The potential of ES cells to transmit the germ line in chimeric mice corresponded to the frequency of cardiomyocyte emergence in the EB outgrowths. We showed that albumin expression data in both emergence and non-

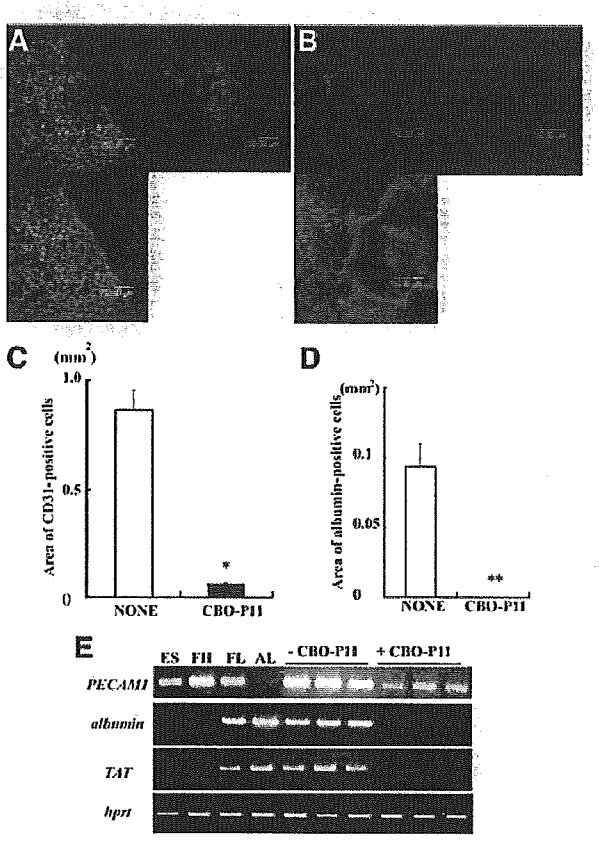

Figure 6. Lack of induction of hepatic morphogenesis by vascular endothelial growth factor inhibitor in the differentiated EBs. **(A, B):** Immunohistochemical analysis of the EB outgrowths at A18 using anti-CD31/PECAM-1 antibody in the presence of 10 μM CBO-P11 for 18 days **(B)** and without CBO-P11 as a control **(A)**. **(C, D):** Quantitative analysis of the CD31/PECAM-1–positive area in the EB outgrowths at A18 was performed using the same method as that for the thalidomide experiments in each of nine individual fields selected from three independent experiments. **(E):** Endothelial cell and hepatocyte-associated gene expression was analyzed by RT-PCR in the thalidomide-treated EB outgrowths at A18. PCR amplification of *PECAM-1* and *TAT* was carried out for 40 cycles. Amplification of albumin was carried out for 30 cycles. Abbreviations: AL, mouse adult liver; EB, embryoid body; ES, undifferentiated embryonic stem cells; FH, mouse fetal heart at E15; FL, mouse fetal liver at E15; PECAM-1, platelet-endothelial cell adhesion molecule-1; RT-PCR, reverse transcription–polymerase chain reaction; TAT, tyrosine aminotransferase.

emergence of cardiomyocytes, as shown in Figure 1B, although cardiomyocyte ablation and blocking cardiomyocyte differentiation experiments are very interesting. However, we consider that subclone screening for the frequency of emergence of cardiomyocytes from the parental murine ES cells would be useful for establishing an in vitro model of hepatic morphogenesis.

The number of albumin-producing cells increased cumulatively in the expanding vascular network area during differentiation to the late stage. It has been clarified that in vitro differentiation of murine ES cells within EBs leads to complex structures that can mimic the normal developmental process of the early embryo, in particular vasculogenesis and hematopoiesis, although no details of liver morphogenesis have been reported [25–27]. Our present results indicated that expansion of the endothelial cell network derived from ES cells plays an important role in the proliferation of hepatocytes and also liver morphogenesis in vitro, reproducing the events that occur in vivo. Furthermore, our liver morphogenesis system does not involve simple coculture of ES cells with endothelial cells prepared from liver sinusoids or blood vessels but is a novel system that utilizes the differentiation of pluripotent ES cells to cardiomyocytes to support subsequent differentiation to endothelial cells and hepatocytes. The interaction between hepatocytes and endothelial cells in liver organogenesis has already been reported by Matsumoto et al. [10]. Our in vitro system for the induction of liver morphogenesis from ES cells closely corresponds to the natural events of liver development that occur in vivo, as shown in Figure 7. Thalidomide, an inhibitor of angiogenesis, inhibited the differentiation and proliferation of CD31/PECAM-1–positive cells in EB outgrowths. However, there is a possibility that thalidomide may have directly suppressed the differentiation of hepatocytes. Therefore, to confirm the crucial role of endothelial cells in hepatic differentiation and maturation, we examined the effect of CBO-P11, a potent VEGF signal-specific inhibitor [28–30], in our culture system. CBO-P11 strongly suppressed the differentiation and proliferation of CD31/PECAM-1–positive cells, corresponding to endothelial cells, during EB differentiation, and consequently, the differentiation of albumin-positive cells, corresponding to hepatocytes, was completely blocked. These results were consistent with the data obtained from the thalidomide experiment.

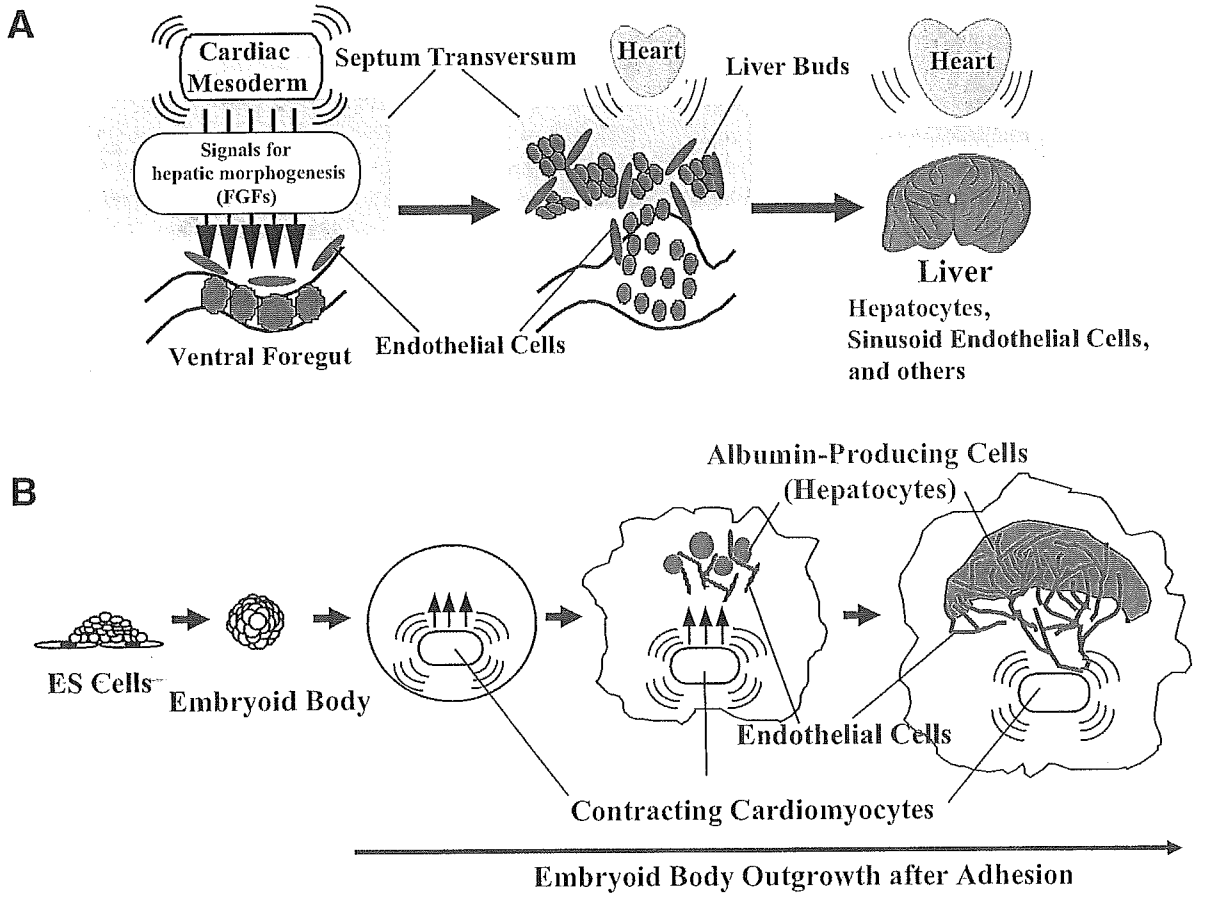

Figure 7. Illustrations of (A) in vivo liver development and (B) our in vitro system for the construction of hepatic organogenesis using murine ES cells. Abbreviations: ES, embryonic stem; FGF, fibroblast growth factor.

The process of organogenesis relies on the presence of specific microenvironments. However, it is difficult to reconstruct such microenvironments in vitro simply by addition of excess free molecules, such as FGF, HGF, and oncostatin M. Strategies for adding growth factors known as liver development inducers to the differentiation medium or for introducing an expression vector of a liver-specific master gene into ES cells can induce the expression of several specific genes in the area of cell interaction, which means that it is difficult to induce the differentiation of ES cell cultures to more than two cell lineages, such as hepatocytes and sinusoidal endothelial cells, through addition of these factors. These kinds of strategies make it impossible, or at least very difficult, to reconstruct target morphogenesis or to induce natural target cells with specific multiple functions. Therefore, no additional growth factors were used in our experiments. We succeeded in reconstructing in vitro the process of liver morphogenesis that involved at least three different types of cell populations: cardiomyocytes, endothelial cells, and hepatocytes. Initiation of liver organogenesis in vivo occurs in the septum transversum. The septum transversum mesenchyme also has important roles in liver organogenesis, such as production of HGF [9, 31]. In our present study, strong expression of HGF was detected in the ES differentiation system, as shown in Figure 2F. Although we detected many fibroblastic cells in this system, it was unclear whether some of these cells corresponded to the septum transversum. With regard to liver function, we were able to demonstrate ammonia degradation activity in this liver differentiation system (Fig. 2G). Unlike a primary hepatocyte culture, which contains almost 100% hepatocytes, our system contains a heterologous population including hepatocytes, endothelial cells, cardiomyocytes, and so on. However, the level of hepatic function, such as ammonia degradation, in each individual hepatocyte was higher in our differentiation system than in a primary culture, suggesting that hepatocyte–endothelial cell contact is very important for the generation of full hepatic function in hepatocytes, as well as for liver development and proliferation in the embryo. Generally, a hepatocyte primary culture has a short life span, shows no proliferation, and has low hepatic function. Therefore, we consider that a hepatocyte primary culture as a single-cell source is not sufficient for creation of a bioartificial liver system and that nonparenchymal cell populations are also necessary for reproducing the complex structure and polarity of the liver seen in vivo.

Here, we established a novel system for liver organogenesis from murine ES cells based on embryological events, i.e., with contributions from cardiac mesoderm and endothelial cell lineages, which were also derived from the ES cells. Furthermore, it has been difficult up to now to culture hepatocytes prepared from adult or embryonic liver in vitro for a long period, as well as to maintain the multiple functions characteristic of the liver. This is one of the major obstacles to the development of a bioartificial liver system. Our system makes it possible to culture ES cell–derived hepatocytes for a long period, at least for more than 30 days, and these cells are able maintain a high degree of hepatic function (Fig. 2F). This innovative system will be useful for creation of liver embryology and regeneration systems as well as for the development of a bioartificial liver system for bridging use in patients waiting for a liver donor and for drug-metabolism assays.

Acknowledgments

We are grateful to Prof. Nobuaki Yoshida and Prof. Yoichiro Iwakura (Institute of Medical Science, University of Tokyo, Toyko) for providing E14.1 ES cells, Prof. Hisato Kondo (Institute for Molecular and Cellular Biology, Osaka University, Osaka, Japan) for NHL7 cells, RIKEN Cell Bank for STO and HePa 1-6 cell lines, and General Research Laboratory, Shinshu University School of Medicine, Nagano, Japan, for technical assistance. This study was supported by grants from the Ministry of Education, Sports, Science and Technology of Japan (Tokyo) (15700314; 13470150, Grant-in-Aid for 21st Century COE program by the above ministry), Hokuto Foundation of Bioscience (Nagano, Japan), and Foundation of Shinshu Igakushinko (Matsumoto, Japan).

References

1 Zaret KS. Regulatory phases of early liver development: paradigms of organogenesis. Nat Rev Genet 2002;3:499–512.

2 Reif S, Terranova VP, el-Bendary M et al. Modulation of extracellular matrix proteins in rat liver during development. Hepatology 1990;12:519–525.

3 Kamiya A, Kojima N, Kinoshita T et al. Maturation of fetal hepatocytes in vitro by extracellular matrices and oncostatin M: induction of tryptophan oxygenase. Hepatology 2002;35:1351–1359.

4 Gualdi R, Bossard P, Zheng M et al. Hepatic specification of the gut endoderm in vitro: cell signaling and transcriptional control. Genes Dev 1996;10:1670–1682.

5 Couvelard A, Bringuier AF, Dauge MC et al. Expression of integrins during liver organogenesis in humans. Hepatology 1998;27:839–847.

6 Jung J, Zheng M, Goldfarb M et al. Initiation of mammalian liver development from endoderm by fibroblast growth factors. Science 1999;284:1998–2003.

7 Fukuda-Taira S. Hepatic induction in the avian embryo: specificity of reactive endoderm and inductive mesoderm. J Embryol Exp Morphol 1981;63:111–125.

8 Douarin NM. An experimental analysis of liver development. Med Biol 1975;53:427–455.

9 Rossi JM, Dunn NR, Hogan BL et al. Distinct mesodermal signals, including BMPs from the septum transversum mesenchyme, are required in combination for hepatogenesis from the endoderm. Genes Dev 2001;15:1998–2009.

10 Matsumoto K, Yoshitomi H, Rossant J et al. Liver organogenesis promoted by endothelial cells prior to vascular function. Science 2001;294:559–563.

11 Sherer GK. Tissue interaction in chick liver development: a reevaluation. I. Epithelial morphogenesis: the role of vascularity in mesenchymal specificity. Dev Biol 1975;46:281–295.

12 Bankston PW, Pino RM. The development of the sinusoids of fetal rat liver: morphology of endothelial cells, Kupffer cells, and the transmural migration of blood cells into the sinusoids. Am J Anat 1980;159:1–15.

13 Enzan H, Himeno H, Hiroi M et al. Development of hepatic sinusoidal structure with special reference to the Ito cells. Microsc Res Tech 1997;39:336–349.

14 Hamazaki T, Iiboshi Y, Oka M et al. Hepatic maturation in differentiating embryonic stem cells in vitro. FEBS Lett 2001;497:15–19.

15 Yamamoto H, Quinn G, Asari A et al. Differentiation of embryonic stem cells into hepatocytes: biological functions and therapeutic application. Hepatology 2003;37:983–993.

16 Yamada T, Yoshikawa M, Kanda S et al. In vitro differentiation of embryonic stem cells into hepatocyte-like cells identified by cellular uptake of indocyanine green. STEM CELLS 2002;20:146–154.

17 Yin Y, Lim YK, Salto-Tellez M et al. AFP(+), ESC-derived cells engraft and differentiate into hepatocytes in vivo. STEM CELLS 2002;20:338–346.

18 Jones EA, Tosh D, Wilson DI et al. Hepatic differentiation of murine embryonic stem cells. Exp Cell Res 2002;272:15–22.

19 Chinzei R, Tanaka Y, Shimizu-Saito K et al. Embryoid-body cells derived from a mouse embryonic stem cell line show differentiation into functional hepatocytes. Hepatology 2002;36:22–29.

20 Lavon N, Yanuka O, Benvenisty N. Differentiation and isolation of hepatic-like cells from human embryonic stem cells. Differentiation 2004;72:230–238.

21 Horai R, Asano M, Sudo K et al. Production of mice deficient in genes for interleukin (IL)-1α, IL-1β, IL-1α/β, and IL-1 receptor antagonist shows that IL-1β is crucial in turpentine-induced fever development and glucocorticoid secretion. J Exp Med 1998;187:1463–1475.

22 Itoh H, Abo T, Sugawara S et al. Age-related variation in the proportion and activity of murine liver natural killer cells and their cytotoxicity against regenerating hepatocytes. J Immunol 1988;141:315–323.

23 Nagy A, Rossant J, Nagy R et al. Derivation of completely cell culture-derived mice from early-passage embryonic stem cells. Proc Natl Acad Sci U S A 1993;90:8424–8428.

24 Auerbach W, Dunmore JH, Fairchild-Huntress V et al. Establishment and chimera analysis of 129/SvEv- and C57BL/6-derived mouse embryonic stem cell lines. Biotechniques 2000;29:1024–1028, 1030, 1032.

25 Wartenberg M, Gunther J, Hescheler J et al. The embryoid body as a novel in vitro assay system for antiangiogenic agents. Lab Invest 1998;78:1301–1314.

26 Hirashima M, Kataoka H, Nishikawa S et al. Maturation of embryonic stem cells into endothelial cells in an in vitro model of vasculogenesis. Blood 1999;93:1253–1263.

27 Wang R, Clark R, Bautch VL. Embryonic stem cell-derived cystic embryoid bodies form vascular channels: an in vitro model of blood vessel development. Development 1992;114:303–316.

28 Bikfalvi A. Recent developments in the inhibition of angiogenesis: examples from studies on platelet factor-4 and the VEGF/VEGFR system. Biochem Pharmacol 2004;68:1017–1021.

29 Bello L, Lucini V, Costa F et al. Combinatorial administration of molecules that simultaneously inhibit angiogenesis and invasion leads to increased therapeutic efficacy in mouse models of malignant glioma. Clin Cancer Res 2004;10:4527–4537.

30 Zilberberg L, Shinkaruk S, Lequin O et al. Structure and inhibitory effects on angiogenesis and tumor development of a new vascular endothelial growth inhibitor. J Biol Chem 2003;278:35564–35573.

31 Andermarcher E, Surani MA, Gherardi E. Co-expression of the HGF/SF and c-met genes during early mouse embryogenesis precedes reciprocal expression in adjacent tissues during organogenesis. Dev Genet 1996;18:254–266.

Lanosterol synthase mutations cause cholesterol deficiency–associated cataracts in the Shumiya cataract rat

Masayuki Mori,[1] Guixin Li,[1] Ikuro Abe,[2] Jun Nakayama,[3] Zhanjun Guo,[1] Jinko Sawashita,[1] Tohru Ugawa,[4] Shoko Nishizono,[5] Tadao Serikawa,[6] Keiichi Higuchi,[1] and Seigo Shumiya[7]

[1]Department of Aging Biology, Institute on Aging and Adaptation, Shinshu University Graduate School of Medicine, Matsumoto, Japan. [2]School of Pharmaceutical Sciences, University of Shizuoka, Shizuoka, Japan. [3]Department of Pathology, Shinshu University School of Medicine, Matsumoto, Japan. [4]Cardiovascular Diseases Research, Yamanouchi Pharmaceutical Co. Ltd., Tokyo, Japan. [5]Department of Nutrition, Faculty of Nursing and Nutrition, Siebold University of Nagasaki, Nagasaki, Japan. [6]Institute of Laboratory Animals, Graduate School of Medicine, Kyoto University, Kyoto, Japan. [7]Department of Laboratory Animal Science, Tokyo Metropolitan Institute of Gerontology, Tokyo, Japan.

The Shumiya cataract rat (SCR) is a hereditary cataractous strain. It is thought that the continuous occurrence of poorly differentiated epithelial cells at the bow area of the lens forms the pathophysiological basis for cataract formation in SCRs. In this study, we attempted to identify the genes associated with cataract formation in SCRs by positional cloning. Genetic linkage analysis revealed the presence of a major cataract locus on chromosome 20 as well as a locus on chromosome 15 that partially suppressed cataract onset. Hypomorphic mutations were identified in genes for *lanosterol synthase* (*Lss*) on chromosome 20 and *farnesyl diphosphate farnesyl transferase 1* (*Fdft1*) on chromosome 15, both of which function in the cholesterol biosynthesis pathway. A null mutation for *Lss* was also identified. Cataract onset was associated with the specific combination of *Lss* and *Fdft1* mutant alleles that decreased cholesterol levels in cataractous lenses to about 57% of normal. Thus, cholesterol insufficiency may underlie the deficient proliferation of lens epithelial cells in SCRs, which results in the loss of homeostatic epithelial cell control of the underlying fiber cells and eventually leads to cataractogenesis. These findings may have some relevance to other types of cataracts, inborn defects of cholesterol synthesis, and the effects of cholesterol-lowering medication.

Introduction

Cataracts, a leading cause of blindness worldwide, represent a multifactorial eye disease. No method apart from surgical intervention has been shown to be effective in halting cataract formation in the lens. Distinct types of cataracts can be defined according to the section of the lens that becomes opaque and the time of onset. Several risk factors for cataract formation have been identified, including increasing age, genetic predisposition, oxidative stress, exposure to UV light and other toxic agents, and diseased conditions such as diabetes.

Animal models have greatly contributed to the study of cataracts (reviewed in ref. 1). The Shumiya cataract rat (SCR) is a hereditary cataractous rat strain (2). SCRs develop mature cataracts at around 11 weeks of age, exhibiting opacity from the perinuclear zone to the cortical intermediate layer (2–4). The morphological mechanism that causes cataract onset is the extension of anterior sutural hypoplasia and liquefied anterior cortical fibers toward the posterior subcapsular region (3, 4). Mild dysplasia of the anterior suture, aggregated epithelial cells overlying the sutural area, and poorly differentiated epithelial cells at the bow area are observable in SCRs from 2 weeks of age (3). The vertebrate eye lens contains only a single layer of epithelial cells on its anterior surface. Lens epithelial cells are essential for maintaining the metabolic homeostasis and transparency of the entire lens, such that it is thought that the continuous occurrence of poorly differentiated epithelial cells at the bow area is responsible for cataract formation in the SCR lens (3). Intriguingly, the lens epithelium is also the initiation site for other types of cataracts, such as selenite-induced cataracts in rabbits (5), UV cataracts in cultured rat lenses (6), rat sugar cataracts (7), and, more importantly, noncongenital cataracts in humans (8).

It is well known that during the development of a mature cataract, degeneration and liquefaction of the remaining lens fibers progresses until the lens becomes liquefied, emulsified, membranous, and finally flattened, leading to a hypermature cataract. However, in the SCR model, following the development of mature cataracts at around 11 weeks of age, normal cortical fibers are regenerated. The lens recovers at around 12 months of age, leaving opacity only in the perinuclear zone (4). This implies that the SCR model may be useful for studies of cataract therapy or even prevention.

The biochemical processes leading to lens opacity have been extensively studied in SCRs, which has revealed upregulation of inducible nitric oxide synthase and elevated calcium influx into lens cells (9), calpain activation (10, 11), and enhancement of proteolysis of crystallins and cytoskeletal proteins (12). Another unique feature in SCRs is the hereditary nature of the condition. Although SCR is an inbred strain, the mean cataract occurrence in progeny of cataractous SCR sib-pairs is about two-thirds, while one-third of progeny remains normal. Necropsy at 21 days after mating reveals that about 25% of the embryos die in utero, so it appears that 1 copy of a recessive gene associated with embryonic

Nonstandard abbreviations used: FDFT1, farnesyl diphosphate farnesyl transferase 1; LSS, lanosterol synthase; SCR, Shumiya cataract rat; U18666A, 3-β(2-diethylaminoethoxy)-androst-5-en-17-one hydrochloride.

Conflict of interest: The authors have declared that no conflict of interest exists.

Citation for this article: *J. Clin. Invest.* 116:395–404 (2006). doi:10.1172/JCI20797.

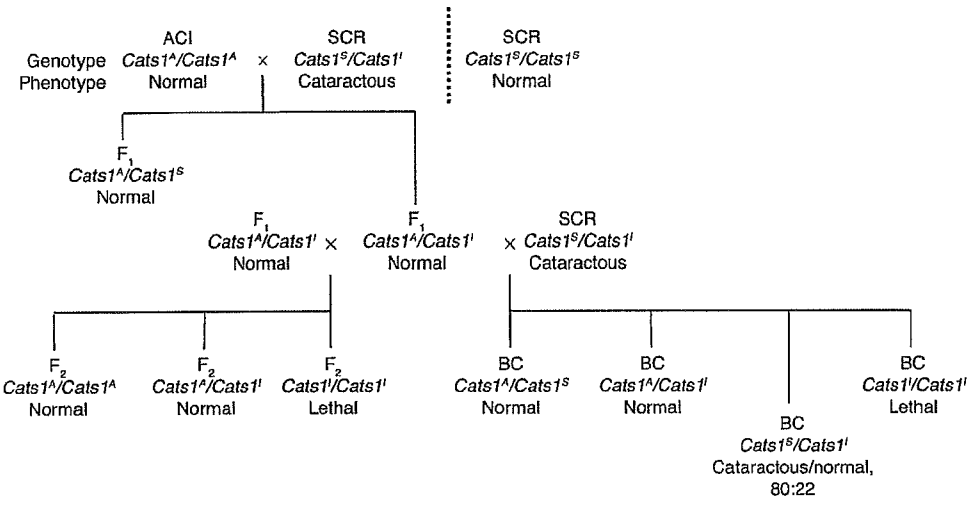

Figure 1
Graphic representation of the rat mating scheme. The test cross to distinguish F_1 rats with and without *Cats1*^{I} is not shown. Putative genotypes were assigned to rats with normal, cataractous, or lethal phenotypes. BC, backcross.

lethality is a prerequisite for cataract onset in SCRs. While subsequent crossing experiments have revealed a second recessive locus essential for cataract onset (2), it remains unclear how the 2 loci interact. Thus, even though the SCR model has been well characterized mechanistically, the primary genetic defect underlying cataractogenesis has not yet been determined. Elucidation of the function of cataract-associated genes would help establish the sequence of biochemical, cellular, developmental, and physiological events that lead from lens epithelial cell damage to cataract formation. To identify such genes, we used positional cloning in the SCR model. Here we show that cataract onset was associated with the specific combination of mutant alleles of *lanosterol synthase* (*Lss*) and *farnesyl diphosphate farnesyl transferase 1* (*Fdft1*) genes, both of which function in the cholesterol biosynthesis pathway. Thus, the SCR model represents a new example of hereditary cholesterol deficiency-associated cataracts. Furthermore our study may have implications for 2 known clinical settings: patients with malformation syndrome due to inborn defects of cholesterol synthesis and individuals taking cholesterol-lowering medication.

Results

A major gene for cataract onset is located on chromosome 20. We performed chromosomal mapping of cataract genes using (SCR × ACI) × SCR backcrosses and (SCR × ACI)F_2 progenies (Figure 1). Eighty of 305 backcross rats developed cataracts by 12 weeks of age. These cataractous rats were genotyped for microsatellite markers. Marker loci on chromosomes 15 and 20 showed significant deviation toward homozygosity for the SCR allele (Figure 2, A and B).

A

Marker locus	Map position	Haplotype
D15Rat137	9.57 cM	S S S H H H H H H S S H
D15Rat83	25.59 cM	S S S S S H H H H H S H
D15Got33	?	S S S S S S H H H H H H
D15Mor3	?	S S S S S S S H H H H H
D15Rat97	41.36 cM	S H S S S S S S H H H H
D15Rat102	58.60 cM	S H H H S S S S S H H H
	n	23 10 4 3 8 1 3 4 4 1 2 17

B

Marker locus	Map position	Haplotype
D20Rat48		S H H S S S S
D20Rat59	4.68 cM	S S H S S S S
D20Rat3	4.68 cM	S S S S S S S
D20Arb4 (Ggtp)	6.90 cM	S S S H S S S
D20Rat60	6.90 cM	S S S H H S S
D20Got7	9.10 cM	S S S H H H S
D20Rat5		S S S H H H H
	n	70 2 1 1 1 3 2

C

Marker locus	Haplotype 1 2 3 4 5 6 7 8
D20Rat59	A A A H S S H H
D20Rat3	A A A H S S H H
D20Arb4 (Ggtp)	A A H H H H S S
D20Rat60	A H H H H H S S
n	40 1 1 77 1 1 1 1

5 6 7 8	Marker locus
S S H H	*D20Rat59*
S S H H	*D20Rat3*
H S H H	*Ftcd*
H H H H	*Lss*
H H S H	*S100b*
H H S S	*Gstt2*
H H S S	*D20Arb4 (Ggtp)*
H H S S	*Gnaz*
H H S S	*D20Rat60*

D

Marker locus	Map position	Haplotype
D15Rat137	9.57 cM	H H S
D15Rat83	25.59 cM	H H H
D15Got33	?	H H H
Fdft1	?	H H H
D15Mor3	?	H H H
D15Rat97	41.36 cM	H H H
D15Rat102	58.60 cM	H S H
	n	13 3 6

Figure 2
Distribution of haplotypes for chromosomes 15 (**A**) and 20 (**B**) observed among 80 cataractous rats from the backcross of (cataractous SCR × ACI)F_1 (putative genotype *Cats1*^{A}/*Cats1*^{I}) × cataractous SCR. (**C**) Distribution of chromosome 20 haplotypes observed among the 123 noncataractous F_2 rats from the cross of (cataractous SCR × ACI)F_1 (putative genotype *Cats1*^{A}/*Cats1*^{I}). The 4 rats homozygous for SCR-derived alleles (haplotypes 5–8) are boxed. A more detailed haplotype of the 4 rats is shown on the right. (**D**) Distribution of haplotypes for chromosome 15 among the 22 normal backcross rats with the *Lss*^{S}/*Lss*^{I} genotype. S, H, and A represent homozygosity for the SCR allele, heterozygosity for the SCR and ACI alleles, and homozygosity for the ACI allele, respectively.

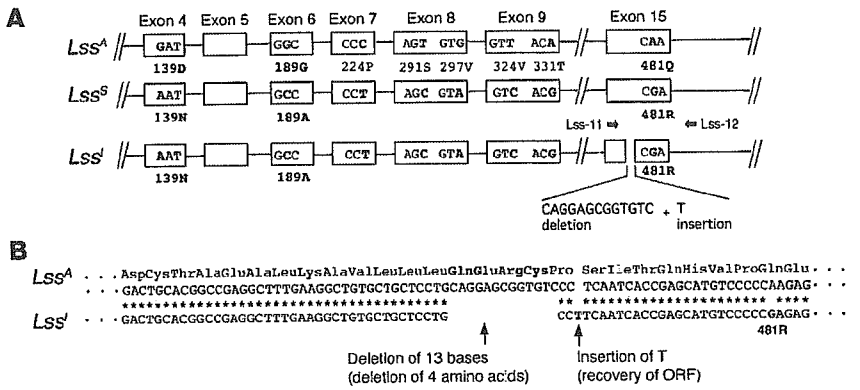

Figure 3
Summary of mutations observed in the rat *Lss* gene. (**A**) Comparison of Lss^A, Lss^S, and Lss^I chromosomal alleles. Eight exonic nucleotide substitutions and the 3 amino acid substitutions are indicated in bold. Approximate positions of primers Lss-11 and Lss-12 used for genotyping are also shown. (**B**) Partial nucleotide sequence of exon 15 of the rat *Lss* gene. The nucleotide sequence of the mutant Lss^I allele is aligned with that of the normal Lss^A allele, with nucleotide matches indicated by asterisks. The Q481R substitution shared with the Lss^I and Lss^S alleles, and the 4–amino acid deletion H469–C472del are indicated in bold.

On chromosome 15, the largest deviation was observed at *D15Mor3* (homozygosity/heterozygosity, 52:28; $\chi^2 = 7.2$; $P < 0.05$). An even larger deviation was observed at *D20Rat3* on chromosome 20 (homozygosity/heterozygosity, 80:0; $\chi^2 = 80.0$; $P < 0.001$), which suggested the nearby presence of a major cataract gene (tentatively designated *Cats1* for cataract Shumiya 1). Haplotype analysis assigned the *Cats1* locus to the region between *D20Rat59* and *D20Arb4*, a microsatellite within the *Ggtp* locus.

Genes for cataract and embryonic lethality are allelic. Intriguingly, none of the 123 (SCR × ACI)F_2 rats developed cataracts by 12 weeks of age. As the backcross data indicated a critical *Cats1* region on chromosome 20, the F_2 rats were genotyped for marker loci on this chromosome. Haplotype analysis indicated that 119 F_2 rats (with haplotypes 1–4; Figure 2C) were clearly homozygous or heterozygous for ACI-derived alleles. Two rats each were homozygous for SCR-derived alleles at *D20Rat3* and *Ggtp* (*D20Arb4*). However, the 2 rats homozygous at *D20Rat3* (haplotypes 5 and 6) were heterozygous at *Ggtp*, and the 2 rats homozygous at *Ggtp* (haplotypes 7 and 8) were heterozygous at *D20Rat3*. It was probable that these 4 rats had lost homozygosity for the region between *D20Rat3* and *Ggtp* due to recombination in the interval between the loci. Thus, no F_2 rat was obtained that was homozygous for SCR-derived alleles between *D20Rat3* and *Ggtp*. Prenatal death caused by homozygosity for an SCR-derived allele within this region may

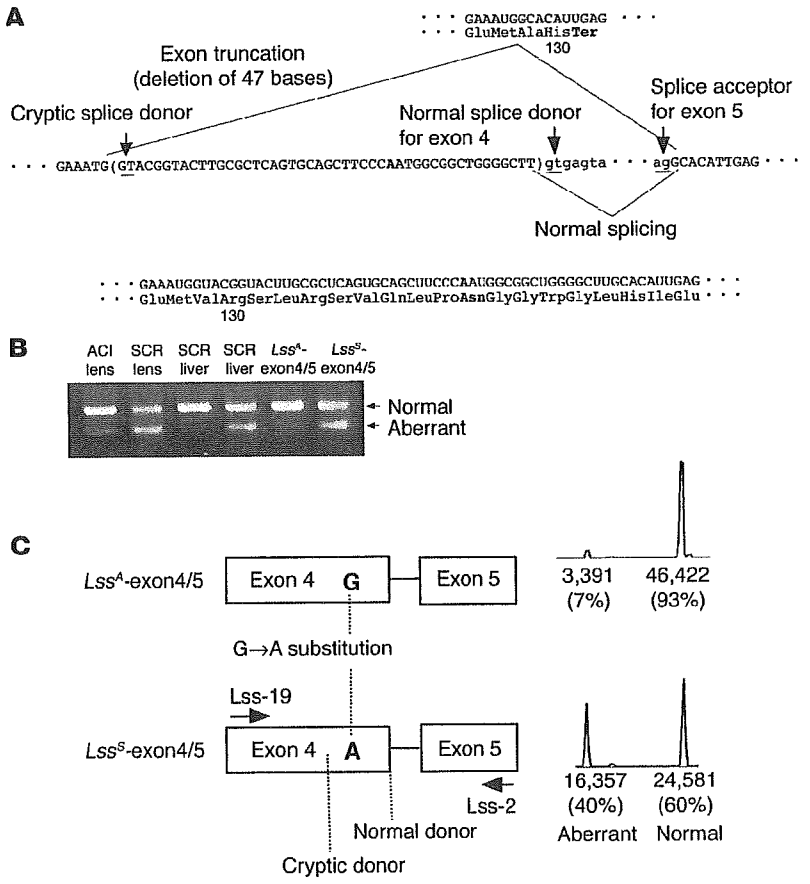

Figure 4
Exon truncation due to a G→A substitution in exon 4 of the rat *Lss* gene. (**A**) Exon and intron sequences are indicated by upper- and lower-case letters, respectively. The A substitution in exon 4 is indicated in bold. The 47 bases deleted by the exon truncation are in parentheses. Also shown are the normal (bottom) and aberrant (top) mRNA sequences and the predicted amino acids. The asparagine substitution at residue 139 is indicated in bold. (**B**) Agarose gel image of RT-PCR products for *Lss* mRNA derived from the livers and lenses of SCR and ACI rats as well as minigene constructs. (**C**) Measurement of aberrant splicing by in vitro transcription of rat *Lss* minigene constructs. Left: Schematic illustrations of the *Lss* minigene constructs. Only inserts in the pEF6/V5-His-TOPO vector are shown. Exons, introns, and primers are not to scale. Arrows indicate oligonucleotide primers. Right: Electropherograms of RT-PCR products from each construct. Peak area values and percentages of total are shown for aberrant and normally spliced products.